Manuscript Details

Manuscript number	MARGO_2018_155_R1
Title	Coupling between tidal mudflats and salt marshes affects marsh morphology
Article type	Research Paper

Abstract

It is generally assumed that coastal salt marshes are capable of adapting to moderately fast rising sea levels although local sediment availability crucially affects this capability. Whilst there is an increasing awareness that the local sediment availability is inherently related to sediment dynamics on the adjacent tidal mudflat, our current understanding of the interactions between salt marshes and tidal flats is very limited. To address this knowledge gap, we measured suspended sediment concentrations alongside hydrodynamic, morphological and sediment deposition measurements over a total period of 16 weeks in a wave-exposed macro-tidal mudflat-salt marsh system on the UK east coast (Tillingham). Our results show that local sediment supply to the salt marsh is strongly linked to intertidal sediment dynamics and that the vast majority of suspended sediment deposited on the marsh originates from wind-wave induced intertidal sediment resuspension in very close vicinity (< 130 m) to the seaward marsh margin. Vertically the salt marsh grows at rates >5 mm yr-1, thereby increasing the slope of the tidal mudflat-salt marsh transition and making the salt marsh susceptible to lateral erosion. Consequently, the marsh edge retreats at a rate of approximately 0.8 m yr-1. Our study shows that the response of coastal salt marshes to climate change is a function of the coupled tidal mudflat-salt marsh system, rather than their vertical sediment accretion rates alone. Therefore, the idea that salt marsh adaptability relies on local sediment supply needs to be expanded, incorporating the morphology and long-term evolution of the adjacent tidal mudflats.

Keywords	Salt marsh, tidal mudflat, sediment deposition, intertidal sediment resuspension, lateral marsh erosion, wave activity
Taxonomy	Salt Marsh, Coastal Process, Intertidal Zone, Geomorphic Change, Erosional Process

Corresponding Author	Mark Schuerch
Corresponding Author's Institution	University of Cambridge
Order of Authors	Mark Schuerch, Tom Spencer, Ben Evans

Suggested reviewers	Ya Ping Wang, Daninka van Proosdij, Rusty Feagin, Nathaniel Weston, Tom Ysebaert, Zeng Zhou

Coupling between tidal mudflats and salt marshes affects marsh morphology

Mark Schuerch[1,2*], Tom Spencer[2], Ben Evans[2]

[1] Lincoln Centre for Water and Planetary Health, School of Geography, University of Lincoln, Brayford Pool Campus, Lincoln, United Kingdom

[2] Cambridge Coastal Research Unit, Department of Geography, University of Cambridge, Downing Place, Cambridge, United Kingdom

*** Correspondence:**

mschuerch@lincoln.ac.uk

Abstract

It is generally assumed that coastal salt marshes are capable of adapting to moderately fast rising sea levels although local sediment availability crucially affects this capability. Whilst there is an increasing awareness that the local sediment availability is inherently related to sediment dynamics on the adjacent tidal mudflat, our current understanding of the interactions between salt marshes and tidal flats is very limited. To address this knowledge gap, we measured suspended sediment concentrations alongside hydrodynamic, morphological and sediment deposition measurements over a total period of 16 weeks in a wave-exposed macro-tidal mudflat-salt marsh system on the UK east coast (Tillingham).

Our results show that local sediment supply to the salt marsh is strongly linked to intertidal sediment dynamics and that the vast majority of suspended sediment deposited on the marsh

originates from wind-wave induced intertidal sediment resuspension in very close vicinity (< 130 m) to the seaward marsh margin. Vertically the salt marsh grows at rates >5 mm yr^{-1}, thereby increasing the slope of the tidal mudflat-salt marsh transition and making the salt marsh susceptible to lateral erosion. Consequently, the marsh edge retreats at a rate of approximately 0.8 m yr^{-1}. Our study shows that the response of coastal salt marshes to climate change is a function of the coupled tidal mudflat-salt marsh system, rather than their vertical sediment accretion rates alone. Therefore, the idea that salt marsh adaptability relies on local sediment supply needs to be expanded, incorporating the morphology and long-term evolution of the adjacent tidal mudflats.

Keywords

Salt marsh, tidal mudflat, sediment deposition, intertidal sediment resuspension, lateral marsh erosion, wave activity

1 Introduction

Coastal salt marshes are increasingly considered as valuable ecosystems at the interface between land and sea; they are known to sequester atmospheric carbon, contribute to global biodiversity, improve coastal water quality, and provide protection against coastal flooding and erosion (Barbier et al., 2011). Under ongoing global sea level rise (SLR; Church et al., 2013) concerns have been expressed, first voiced by Stevenson et al. (1986), that coastal salt marshes may experience 'accretionary deficit' (i.e. not being able to sufficiently adapt their elevation through vertical sediment accretion), become inundated permanently and convert to open water (Crosby et al., 2016; Spencer et al., 2016; Schepers et al., 2017). However, the increase in surface elevation, particularly of minerogenic coastal salt marshes (i.e. salt

41 marshes ‘dominated by tidally introduced mineral matter’ (Allen, 2000)), is driven by the
42 deposition of suspended sediment during inundation events. This process may accelerate
43 under increased rates of SLR and associated higher inundation frequencies (Kolker et al.,
44 2010; Hill and Anisfeld, 2015). The environmental variables primarily controlling the ability
45 of minerogenic coastal salt marshes to vertically adapt to SLR are commonly assumed to be
46 local tidal range, sediment availability and inundation frequency (French, 1993; French,
47 2006; Kirwan et al., 2010; D'Alpaos et al., 2011; Schuerch et al., 2013; Schuerch et al., 2018).

48 It has been variously hypothesised that increased local tidal range will (i) increase sediment
49 resuspension through higher tidal current velocities, hence improving sediment availability
50 (Friedrichs and Perry, 2001; Temmerman et al., 2003; Schuerch et al., 2013); (ii) reduce
51 SLR-induced channel erosion, due to a proportionally smaller increase of the tidal prism
52 (Kirwan and Guntenspergen, 2010); and (iii) increase the elevation range where salt marsh
53 vegetation can grow (Friedrichs and Perry, 2001; Kirwan and Guntenspergen, 2010). Greater
54 sediment availability, seen in higher suspended sediment concentrations (SSCs), will
55 increase the amount of mineral sediment being deposited on the marsh surface during a single
56 inundation (French, 1993; French, 2006; Kirwan and Murray, 2007), assuming an invariant
57 sediment trapping efficiency (i.e. ‘percentage of the sediment introduced on flood tide
58 retained on the marsh surface’ (French, 2006: p. 127)). Finally, it can be argued that if the
59 marsh is inundated more regularly, sediment deposition events will become more frequent
60 and thus the rate of sedimentation will increase.

61 Supply of suspended sediment for coastal salt marshes is highly variable in space and time,
62 owing to the multitude of processes involved in coastal sediment transport and sediment
63 resuspension (Wang et al., 2012), as well as the large variability associated with

meteorological and climate drivers (Schuerch et al., 2016; Zhou et al., 2016; Ma et al., 2018). Despite knowledge about the crucial importance of sediment supply and its pronounced temporal variability for minerogenic marshes, most model-based assessments on the ability of coastal wetlands to adapt to future SLR assume a constant sediment supply (French, 1993; French, 2006; Mariotti and Fagherazzi, 2010; D'Alpaos et al., 2011; Mariotti and Carr, 2014; Rodríguez et al., 2017). Where temporal variations in sediment supply are accounted for, sediment supply is assumed to be driven by current-induced intertidal sediment resuspension (Temmerman et al., 2003; D'Alpaos et al., 2007; Schuerch et al., 2013). However, other studies have suggested that wave-induced sediment resuspension may be more important for marsh sediment supply (Callaghan et al., 2010; Ma et al., 2018) but field data on how wave-induced sediment resuspension affects the morphological development of salt marshes are rare. Furthermore, in order to improve our understanding of the impacts that temporal variations in sediment supply may have on the ability of coastal salt marshes to adapt to future SLR, exact knowledge on the sources of the supplied sediment is necessary, including the relative contributions from both wave- and current-induced sediment resuspension (Schuerch et al., 2014).

It has previously been argued that the sources of mineral suspended sediment supplied to a salt marsh can broadly be divided into external (‘far field’) and proximate (‘near field’) sediment sources (Schuerch et al., 2014). External sediment sources include contributions from riverine sediment discharge (Bergamino et al., 2017), coastal erosion along neighbouring coastlines, offshore sediment sources and atmospheric deposition (Pedersen and Bartholdy, 2006; Schuerch et al., 2014; Schuerch et al., 2016). Proximate sediment sources include sediment resuspension on tidal mudflats and erosion of marsh cliffs and tidal

87 creeks (Friedrichs and Perry, 2001; Pedersen and Bartholdy, 2006; Mariotti and Carr, 2014;
88 Schuerch et al., 2014).

89 The aim of this study was to identify the role of intertidal sediment resuspension in
90 contributing sediment to a salt marsh on the UK east coast from an adjacent, proximate
91 mudflat. Further, we aimed to identify the drivers of temporal variations in intertidal sediment
92 resuspension, particularly focusing on changes in hydrodynamic and meteorological
93 conditions, and to assess how these variations influence sediment deposition processes on
94 the marsh platform. More specifically, the research questions to be answered include: (i) what
95 are the drivers for the temporal variability in sediment supply?; (ii) how does this observed
96 temporal variability affect sediment deposition patterns on the salt marsh platform?; and (iii)
97 what are the implications of the observed temporal variability for the long-term
98 morphological development of the salt marsh?

99 **2 Regional Setting**

100 The study site is a macro-tidal salt marsh on the UK east coast between the Blackwater and
101 the Crouch estuaries (Dengie Peninsula) on the northern margin of the Greater Thames
102 Estuary, near the village of Tillingham (Fig. 1). The mean spring tidal range is 4.8 m, and the
103 neap tidal range 2.9 m (Towler and Fishwick, 2017). This open coast marsh is exposed to a
104 moderate wave climate with a mean significant wave height of 0.18 m and a maximum
105 significant wave height of 0.73 m (October 2012 – July 2016), as measured at the marsh edge
106 (unpublished data).

107 The salt marsh is located to seaward of an earthen embankment (seawall) and has varying
108 widths of up to 700 m. Adjacent to the vegetated marsh platform, an extensive tidal mudflat

extends into the North Sea for up to 3.7 km offshore (Möller, 2006). The transition zone from tidal mudflat to vegetated salt marsh is characterised by a shore-normal system of ridges and runnels (Fig. 2). The elevations of the marsh platform range from 1.9 m in the pioneer vegetation zone to 2.5 m above Ordnance Datum Newlyn (ODN; where 0.0 ODN approximates mean sea level) in the mid and high marsh vegetation zones (Fig. 2).

3 Materials and Methods

3.1 Experimental setup

Field measurements of the hydrodynamics and the morphological development of the tidal mudflat; SSCs along a 177 m long, shore-normal transect; and sediment deposition on the marsh platform were conducted over a 5-week period in summer (25/05 - 28/06/2016) and an 11-week period in autumn/winter (20/09 - 06/12/2016). The most seaward-located measuring station was 130 m from the edge of the vegetated marsh platform (marsh edge) on the tidal mudflat (ASM2113). The most landward location was situated in the mid marsh vegetation zone (a mixed canopy dominated by *Puccinellia maritima*), 47 m inland from the marsh edge and 210 m seaward of the seawall (Fig. 2).

3.2 Hydrodynamic measurements

Water levels along the entire transect were measured using four pressure sensors (Solnist Levellogger, Model 3001), programmed to record water levels every 30 seconds (Fig. 2). The measured raw data from the pressure sensors were corrected for variations in atmospheric pressure and smoothed with a 15-min moving average filter to derive still water levels, maximum inundation depths of tidal inundations (HW levels), tidal asymmetry (i.e.

ebb duration/flood duration) and the frequency of inundation of the marsh surface at the marsh edge (ASM2115). Based on the unsmoothed water levels, and using the method of Reef et al. (2018), the temporal variability in wave activity during the experiment was approximated with a wave proxy, calculated as the tide-averaged absolute water level deviations from the still water level.

The data collected at a recording frequency of 4 Hz by the bottom-mounted PDCR 1830 pressure transmitter (GE Druck) during the high-water stages of selected tidal inundations (Fig. 2) were processed to produce summary wave parameters, following the methodology of Möller et al. (1999). From these wave parameters, the root mean square wave height (H_{rms}) was used to calibrate the wave proxy. The calibration showed that the wave proxy (WP), calculated at ASM2113, was linearly correlated with H_{rms}, recorded by the PDCR 1830. The linear regression showed that $H_{rms} = 6.645 * WP$ ($R^2 = 0.93$), as reported by Reef et al. (2018).

Tidal currents were measured on the tidal mudflat at ASM2113, using an Acoustic Doppler Current Profiler (ADCP), namely an Aquadopp Profiler 2 MHz (Nortek AS), with a recording interval of 30 s. Various measurement settings were tested to optimize the measurement accuracy and precision, including cell size and measurement load (ping rate). The resulting measurement precision typically ranged between 1 and 2 cm s^{-1} with a nominal accuracy of 0.5 cm s^{-1} (Nortek technical specification).

3.3 Turbidity measurements

Turbidity measurements were conducted using two turbidity profilers, namely two Argus Suspension Meters (ASM) IV (ARGUS Gesellschaft für Umweltmeßtechnik mbH). The profilers consist of 144 optical backscatter sensors, arranged as a vertical array with a spacing

of 1 cm. One turbidity profiler (ASM2113) was deployed on the mudflat (130 m from the marsh edge); the other (ASM2115) was located in the transition zone between the annual pioneer vegetation and the perennial marsh vegetation, the boundary defined as the marsh edge for the purpose of this experiment (Fig. 2). Data were recorded every 30 seconds, averaging 10 measurements at 1 Hz within 10 s. All measurements were discarded when inundation depths were lower than 3 cm.

Conversion of the turbidity data (ftu) to SSC (mg l^{-1}) was performed based on 53 1-litre water samples, collected with an automated water sampler (Teledyne ISCO, model 6712) during three time periods in April (7 - 11), July (21 - 24) and December (12 - 17) 2016. Water samples were filtered using pre-weighed GF/C filters, dried at 105°C for 24 hours and subsequently re-weighed. For the 5-week measurement period in summer, the SSCs derived from 34 water samples from April and July were used for the instrument calibration (Reef et al., 2018); for the autumn and winter measurement period, the SSCs derived from 19 water samples from December were utilized (unpublished data).

3.4 Measurements of sediment deposition on the salt marsh surface and elevation change

Sediment deposition was measured using filter traps, deployed on the marsh surface at three different locations along a cross-shore transect, starting from the landward turbidity profiler (ASM2115) and proceeding in a landward direction (Fig. 2). During the summer period, measurements were conducted at the sites ASM2115, P4 and SET1, whereas during the autumn/winter period, the site SET1 was exchanged for SET2 (Fig. 2). At each location, three filter traps were installed to capture the small-scale spatial variability in deposition and to

derive an average local deposition. The filter traps consisted of pre-weighed glass-fibre filters (Whatman GF/F) with a diameter of 9 cm, being placed on an equally sized petri dish and fixed with three metal pegs (Nolte et al., 2013). Following their deployment, the filter traps were usually retrieved after five days, although retrievals varied between two and ten days.

Alongside the transect of filter traps, a Rod Surface Elevation Table (RSET; Cahoon et al., 2002), was used in combination with feldspar marker horizons (MH) at two different sites (SET1 and SET2, figure 2) to monitor surface elevation changes and sediment accretion rates between December 2015 and February 2017, with measurements on 18 December 2015, 11 July 2016 and 17 February 2017. In contrast to the filter traps, the coupled RSET and MH method reveals the longer-term salt marsh surface elevation change and near-surface vertical accretion rate respectively (Cahoon et al., 1995). Average surface elevations and standard deviations were calculated from 36 measurements for each RSET site, consisting of nine measurements at four locations around the site. Similarly, average accretion rates and standard deviations were calculated from 12 MH measurements per site, namely three replicates at four locations around the site (same locations as used for the RSET measurements).

3.5 Measurement of mudflat surface elevation

The sediment dynamics on the tidal mudflat were monitored using coloured sand tracer sticks that were vertically inserted into the mudflat, until the upper end of the column was level with the mudflat surface. The tracer sticks (88 mm in length, 10 - 20 mm in width, 5 - 10 mm in thickness) consisted of a mixture of coloured sand and a highly concentrated sugar solution, which were “baked” in a plastic tray for three days at 50°C. Upon insertion into the

196 mudflat, the solidified sand tracers, cemented by the sugar solution, dissolved as the sugar
197 solution dissolved in the water-saturated sediment, and the coloured sand was left as an
198 indicator for sediment mobilization and deposition (Runte, 1989; Schwarzer et al., 2003). In
199 contrast to the tidal mudflat under investigation, the tracer sticks consisted of non-cohesive
200 sand particles to ensure rapid dissolution of the binding material (the sugar solution).
201 Meanwhile, the effect of the potentially higher erodibility is of the tracer stick material was
202 counteracted by the small width and thickness of the tracer stick.

203 After five days (occasionally two or ten days), a 20 cm long sediment core was extracted at
204 each tracer location, using a PVC tube with an inner diameter of 7.0 cm, to retrieve the
205 remaining tracer stick. In the laboratory, each core was opened through its centre to measure
206 the remaining length of the tracer stick (L) as well as the thickness, if any, of the sediment
207 layer deposited above the tracer (T). . The net erosion (E = negative) or deposition (E =
208 positive) was calculated based on the initial length of the tracer stick (IL): $E = IL - (L + T)$.

209 **3.6 Meteorological data**

210 Meteorological data (recorded wind speeds and wind directions) for the time period of the
211 experiment were obtained from the weather station at Shoeburyness, Thames Estuary (Met
212 Office, 2006), 17 km SE of the study site (Fig. 1). It was assumed that the study site was
213 exposed to the same wind condition as at Shoeburyness.

214 **3.7 Long-term marsh edge dynamics**

215 The overall change in marsh edge position was determined for the time period 1992 to 2013
216 over the 11 km long eastward facing edge of the Dengie Peninsula that is fronted by marsh.

The seaward limit of macrophytic vegetation was manually digitised from UK Environment Agency vertical aerial photography for both years (25 cm resolution panchromatic in 1992 and 20 cm RGB in 2013, late summer acquisitions). The Digital Shoreline Analysis System (DSAS; Thieler et al., 2009) was then used to cast shore-normal transects at 10 m alongshore spacing and calculate the rate of change (Net Shoreline Movement (NSM; m)) at each transect intersection with the digitised shorelines. Transects where shoreline change resulted in a transect crossing a creek between intersections with the two shorelines were discarded. A total of 1058 transects were retained for analysis.

3.8 Statistical methods

The hydrodynamic forcing and the turbidity data (water level, wave activity and SSC) were aggregated for each tidal inundation as well as for each sampling period of the measurements on marsh and mudflat morphodynamics (Table 1). This enabled us to directly relate the hydrodynamic forcing to the data collected on the morphological responses of the salt marsh and the mudflat, for time periods of between 2 and 10, but usually 5, days.

The statistical analyses of the collected data included:

(i) Identification of drivers for intertidal sediment resuspension: (non-) linear regression analysis between the median SSC (per tide) at ASM2113 and the hydrodynamic forcing (table 1).

(ii) Comparison between landward and seaward turbidity sensors: linear regression analysis between median SSC (per tide) at ASM2113 and ASM2115.

(iii) Identification of drivers for the observed differences: stepwise linear regression analysis with SSC difference (per tide) as the dependent variable and all variables for hydrodynamic forcing (table 1) as independent variables.

(iv) Analysis of drivers for temporal variability of average sediment deposition on the salt marsh (per sampling period): stepwise linear regression analysis with average sediment deposition as dependent variable and SSC variables (table 1) plus inundation frequency (IF) at ASM2115 as independent variables.

(v) Trend analysis of the spatial patterns of sediment deposition, averaged over the entire experiment using boxplots and the non-parametric Kruskal-Wallis test.

(vi) Identification of significant trends for sediment deposition as a function of distance from the marsh edge: (a) linear regression analysis to test for a significant ($p < 0.05$) linear (positive or negative) trend; (b) nonlinear regression analysis for all insignificant periods testing for a significant (convex or concave) 2^{nd} order polynomial relationship.

(vii) Analysis of drivers for spatial sediment deposition patterns (as identified in (vi)): non-parametric Kruskal-Wallis test applied to all variables for hydrodynamic forcing and turbidity (table 1), categorized based on the identified spatial sediment deposition patterns.

Following every stepwise linear regression analysis, all variables included in the resulting regression models were tested for correlation (Pearson correlation coefficient). Where model variables were significantly correlated ($p < 0.05$), the variable with the higher p-value was removed from the model and the stepwise linear regression was repeated until all model variables were independent from each other.

4 Results

4.1 Hydrodynamic forcing

The entire measurement period included seven complete spring-neap tidal cycles. These were characterized by higher neap high water (HW) levels and lower spring HW levels during the summer period and lower neap HW levels combined with higher spring HW levels during the autumn and winter. While the seaward turbidity profiler (ASM2113) was inundated on every tide, the landward profiler (ASM2115) was only inundated during tides exceeding 1.2 m inundation depth at ASM2113. The average inundation depth at ASM2113 was 1.28 m, with a maximum of 2.13 m during the first tidal inundation on 17/11/2016 and a minimum of 0.38 m during the first tide on 11/10/2016. Tidal flow velocities on the mudflat (at ASM2113) were very low and could not be determined using the instrument's precision of 1-2 cm s^{-1} and its accuracy of 0.5 cm s^{-1}.

Although, the wave activity measured at ASM2113 was not correlated with the measured HW levels (Pearson's r = -0.1043, p = 0.14), the maximum wave activity appeared to be related to inundation depth, with higher waves possible when inundation depths were large. The upper boundary values of the measured wave proxy (WP_{max}) thereby appeared to follow a linear relationship with inundation depth (h): $WP_{max} = 0.045 * h$.

Wave activity in summer was not significantly different (Kruskal-Wallis: p = 0.79) from wave activity in autumn/winter (WP = 0.022 in summer, compared to 0.023 in winter). The maximum wave activity in summer (WP = 0.058) was recorded during the first tide on 02/06/2016, whereas the maximum wave activity in autumn/winter (WP = 0.064) occurred during the first tide on 20/11/2016. Sustained periods (> 2 days) of increased wave activity

(*WP* >0.025), identified using a smoothed *WP* time series (moving average: window size of 10 tides), were 24/05 - 05/06/2016, 03/10 - 08/10/2016, 11/10 - 16/10/2016 and 18/11 - 28/11/2016.

The measured wave proxy was significantly correlated with the recorded wind speed (v, knots) and wind direction (θ in degrees azimuth) at Shoeburyness. Higher wind speeds created higher waves when blowing onshore and lower waves when blowing offshore:

$$WP = m * [v * \sin((\theta * 180)/\pi) + 1.4)] + a \qquad \text{(equation 1)}$$

where $m = 0.000879$ is the slope and $a = 0.0125$ the intersect of the linear regression between the sinus-transformed wind speed (term within square brackets) and the wave proxy ($R^2 = 0.54$, $p < 0.001$).

4.2 Suspended sediment concentrations

On the tidal mudflat (ASM2113) the median depth-averaged SSC ranged from 0.03 to 279 mg l^{-1} in summer and from 2.6 to 1039 mg l^{-1} in autumn/winter. In both seasons SSC showed a strong positive relationship with wave activity. In autumn/winter, strong wave activity had a greater impact on SSC than in summer (Fig. 3). The relationship between the wave proxy and the median depth-averaged SSC followed a linear trend in summer ($R^2 = 0.72$) and a power function in winter ($R^2 = 0.77$) as a best fit (Fig. 3).

The highest SSC at ASM2113 (1039 mg l^{-1}) was recorded for the first tide on 22/11/2016 during a period of three days (20/11 - 22/11/2016) when the median SSC was greater than 900 mg l^{-1} for every tidal inundation. During the same time period, the highest SSC was also recorded at the landward turbidity profiler, located at the marsh edge (ASM2115). At this

location the maximum SSC was 1445 mg l^{-1}. Generally, the SSC records at ASM2113 (mudflat) and ASM2115 (marsh edge) were significantly correlated with each other (R^2 = 0.83, p <0.001). However, on average, SSC at the marsh edge was 25% higher than on the mudflat (Fig. 4), indicating a general landward increase in SSC. The general trend towards a landward increase in SSC was also represented in the median concentrations of 42 and 74 mg l^{-1} for the sensors on the mudflat and at the marsh edge respectively.

The greatest difference between the landward and the seaward sensors (i.e. landward increase in SSC) was observed during the first tide on 20/11/2016, when SSC at the landward sensor was 519 mg l^{-1} higher than on the mudflat. Meanwhile, the largest difference for the summer period was recorded for the first tide on 31/05/2016. Comparing the differences in SSC between the landward (ASM2115) and the seaward (ASM2113) sensors with the hydrodynamic forcing (i.e. HW level, wave proxy, depth-normalized wave proxy at ASM2113), the depth-normalized wave proxy (WP_{norm}) best explained the observed variations (R^2 = 0.22, p <0.0001). Moreover, the upper boundary of the landward sediment transport (y_{max}) was defined by WP_{norm} (y_{max} = 16000 * WP_{norm}).

4.3 Sediment deposition

4.3.1 Temporal sediment deposition pattern

The average sediment deposition (g) on all filter traps during the measurement period ranged between 0.03 and 1.30 g, averaging 0.40 g per sampling period. The highest sediment deposition took place between 24/05 and 3/06/2016 (1.11 g) in summer and between 15/11 and 21/11/2016 (1.32 g) in autumn/winter. Interestingly, the sediment deposition in summer

was not significantly (Kruskal-Wallis: $p = 0.93$) different from that in autumn/winter, although the median and the maximum deposition were higher (Fig. 5).

The average sediment deposition appeared to be significantly correlated with the maximum SSC at the landward sensor (ASM2115), and the number of inundations during each sampling period (inundation frequency). The linear regression model including these two parameters explains 69% of the observed variability in sediment deposition (Fig. 5). While representing the more important driver for sediment deposition on the marsh, the maximum SSC at ASM2115 (C_{max}) appeared to be linearly related to the maximum increase in SSC between the seaward and the landward turbidity sensors (max. landward SSC increase: C_{diff}): $C_{max} = 2.02 * C_{diff} + 77.9$ ($R^2 = 0.66$, $p < 0.001$).

4.3.2 Spatial sediment distribution pattern

Averaged over the entire measurement period, the sediment deposition recorded on the filter traps at the different locations within the marsh did not significantly differ between each other (Kruskal-Wallis: $p = 0.23$), suggesting no systematic differences between the different sites, and most importantly, no landward decrease in sediment deposition (Fig. 6).

The trends for sediment deposition as a function of distance from the marsh edge for every sampling period individually are shown in Figure 7. A significant linear decrease from the marsh edge inland was only observed between 21/11 and 26/11/2016, whereas a linear increase was observed for two sampling periods (03/06 - 08/06/2016 and 10/11 - 15/11/2016). During four sampling periods, we found a polynomial rather than a linear sedimentation pattern. The maximum sediment deposition was measured in the centre of the marsh (concave polynomial pattern) during the two sampling periods 20/09 - 24/09/2016 and

346 24/09 – 04/10/2016, whereas the minimum sediment deposition was in the centre of the
347 marsh (concave polynomial pattern) during the sampling periods 09/10 - 19/10/2016 and
348 15/11 - 21/11/2016. However, for most sampling periods we could not determine any
349 significant linear or polynomial trends (Fig. 7); and the observed spatial distribution patterns
350 were not significantly related to any hydrodynamic forcing or turbidity variable (Table 1).

351 **4.4 Mudflat morphology**

352 On the mudflat, adjacent to the salt marsh, net erosion was the dominant process observed
353 during the measurement period (Fig. 8), although the difference between summer and winter
354 erosion was insignificant (Kruskal-Wallis: $p = 0.23$). However, the strongest erosion events
355 were recorded in autumn/winter, namely between 21/11 and 26/11/2016 (1.5 cm, on average)
356 and between 4/10 and 9/10/2016 (1.0 cm, on average). These periods coincided with the two
357 periods showing the highest average wave proxy during the entire measurement period (Fig.
358 8). Meanwhile, net sediment deposition was observed during two periods only, namely
359 between 14/10 and 21/10/2016 (1 cm, on average) and between 10/11 and 15/11/2016 (0.6
360 cm, on average). Both of these periods were characterized by relatively high maximum tidal
361 HW levels, i.e. two of the four highest inundation periods show net deposition (Fig. 8).
362 However, none of the data series for HW levels (average and maximum HW levels), wave
363 activity (average and maximum wave proxy) and sediment resuspension (average and
364 maximum SSC at ASM2113) were significantly correlated with the measured mudflat
365 erosion (Fig. 8).

366 **4.5 Surface elevation change and vertical accretion**

367 Surface elevation change over the period of our experiment was 5.6 ±1.5 (1 (standard
368 deviation) mm yr^{-1} at SET1 and ca. 5.3 ±2.3 mm yr^{-1} at SET2 (Table 2: RSET rates).

Meanwhile, the sediment accretion rates were 17.4 ±2.4 and 9.0 ±2.8 mm yr^{-1} for the marker horizons (MH) at SET1 and SET2 respectively (Table 2: MH rates). These differences indicate that so-called 'shallow subsidence' (Cahoon et al., 1995), caused by sediment autocompaction (i.e. difference between MH and RSET rate), is much higher at site SET1 compared to site SET2. This enhanced compaction may be related to the closer vicinity of SET1 to the tidal creek network and the better drainage of the site, leading to higher invertebrate activity and greater void space below the SET1 surface. Additionally, the redox environments may be more favourable to decomposition of organics where oxygen availability is higher. Long-term marsh edge dynamics

Margin retreat was found to be near-ubiquitous for the entire Dengie Peninsula with a mean rate of 1.93 m yr^{-1}. For the 60 m of marsh margin centred on the measurement transect, the 1992 - 2013 mean rate of retreat was 0.80 m yr^{-1} (standard deviation 0.23 m yr^{-1}). The region of maximum retreat (regularly exceeding 5.50 m yr^{-1}) was 1 km south of the study transect.

5 Discussion

5.1 Drivers of intertidal sediment resuspension

The supply of sediment as a vital control on the ability of coastal salt marshes to adapt to rising sea levels has widely been acknowledged in previous studies (Reed, 1989; French, 1993; French, 2006; Blum and Roberts, 2009; Weston, 2014). This study, conducted at a wave-exposed, macro-tidal coastal salt marsh on the UK east coast, shows that sediment availability of salt marshes is subject to pronounced temporal variability, with major variations in SSC on diurnal time scales. In contrast to systems dominated by tidal currents (e.g. Scheldt estuary: Fettweis et al., 1998; Severn estuary: Allen and Duffy, 1998), sediment supply on this marsh is primarily controlled by wave-induced sediment resuspension(Fig. 3),

392 rather than resuspension caused by tidal currents, which were shown to be slower than the
393 detection limit our ADCP. Wave-induced sediment resuspension is triggered when the wave-
394 induced bed shear stress exceeds the critical bed shear stress of the mudflat surface, a
395 condition that is more likely to be met in shallow water conditions (Green and Coco, 2014).

396 In addition, the impact of wave activity on intertidal sediment resuspension varies seasonally,
397 leading to higher SSCs in winter than in summer (Temmermanet al., 2003; Poirier et al.,
398 2017). The weaker effect of wave activity on sediment resuspension during the summer
399 months (Fig. 3) is likely related to the presence of seasonal biofilms (Underwood and
400 Paterson, 1993; Paterson et al., 2000; Andersen, 2001; Tolhurst et al., 2008; Grabowski et
401 al., 2011) and/or macroalgal mats (Frostick and McCave, 1979) covering the tidal mudflat,
402 thereby reducing the erodibility of the mudflat surface.

403 Comparison of the seaward and landward turbidity during our experiment revealed a
404 landward increase in SSC, indicating sediment resuspension in the near-salt marsh margin
405 zone and subsequent landward sediment transport. This transport was significantly related to
406 the depth-normalized wave activity, suggesting that waves initiate sediment resuspension and
407 landward transport, particularly when water levels are low. Meanwhile, tidal currents appear
408 not to play a significant role in onshore sediment transport, as they are of low magnitude
409 compared to the prevailing wave activity. Similar wave-induced landward sediment transport
410 has recently been reported for the Oosterschelde, NL (Ma et al., 2018). However at other
411 sites, tidal currents have been shown to have a greater impact on landward sediment transport
412 than wave activity (Janssen-Stelder, 2000; Zhu et al., 2014). Furthermore, some studies have
413 emphasized the importance of longshore and cross-shore sediment advection for SSC and
414 tidal mudflat topography (Wang et al., 2012; Shi et al., 2016). However, these advection

terms have been shown to be most pronounced in the lower (seaward) parts of tidal mudflats (Le Hir et al., 2000; Wang et al., 2012), with wind and current-induced sediment resuspension becoming more important towards the upper (landward) part of the tidal mudflat (Green, 2011; Ma et al., 2018). The latter position is where our measurements took place.

In previous studies, the erosion of tidal mudflats due to wave activity has widely been attributed to strong wind and storm events, with calm weather periods being responsible for intertidal sediment accretion, creating an equilibrium profile, adjusted to the prevailing wind and tide conditions (Janssen-Stelder, 2000; Le Hir et al., 2000). The data reported here, however, show little sign of elevation increases of the tidal mudflat during calm weather periods, and bed level changes are not significantly related to wave activity, a finding that is confirmed by recent data on mudflat elevation changes in various marsh system across the North Sea (Willemsen et al., 2018). The dominant signal is one of surface lowering, suggesting that the mudflat is out of equilibrium with prevailing energy conditions.

5.2 Sediment deposition on the marsh surface

The temporal variability of sediment deposition on the salt marsh surface was remarkably well correlated with the maximum SSC at the marsh edge and the inundation frequency of the marsh during each sampling period; when combined, these two variables explained 69% of the observed temporal variability in sediment deposition on the salt marsh. The maximum SSC for each sampling period thereby appears to be more important for surface deposition than the average SSC. Similar to previous studies on the vertical accretion of micro- and meso-tidal marshes (Bartholdy et al., 2004; Bellucci et al., 2007; Schuerch et al., 2013), this finding suggests that frequently occurring moderate to strong wind events, rather than extreme events or everyday tidal inundations, primarily control salt marsh sedimentation, at

438 least in more seaward marsh locations. By contrast, in macro-tidal marshes, extreme storm-
439 events have been shown to be more important for the vertical accretion of higher, interior
440 marsh areas (French and Spencer, 1993; van Proosdij et al., 2006).

441 Given that the maximum SSC at the marsh edge is strongly related to the maximum increase
442 in SSC between the turbidity sensors on the mudflat and at the marsh edge ($R^2 = 0.66$), the
443 majority of the sediment delivered to the salt marsh must originate from the zone extending
444 up to 130 m from the marsh edge, either from the tidal mudflat or the marsh edge (i.e. the
445 shore-normal ridge and runnel system) itself.. The narrowness of this zone is remarkable,
446 given that the tidal mudflat adjacent to the this part of the salt marsh extends seaward for3.7
447 km. The exact relative contributions of sediment supplied from the erosion of the ridge and
448 runnel system compared to sediment supplied from the erosion of the tidal mudflat cannot as
449 yet be quantified. Our data, however, indicates a contribution from both source areas.

450 The removal of sediment from this area of the tidal mudflat during increased wave activity
451 is also supported by the observed predominant lowering of the mudflat surface between the
452 seaward and the landward turbidity sensors. However, unlike earlier suggestions (Le Hir et
453 al., 2000), we show that much of this sediment is not removed from the system but
454 transported landward onto the adjacent salt marsh where it is deposited. Also, the sediment
455 seems not to originate from the marsh edge only, as previously suggested (Reed, 1988);
456 rather, the removal of the sediment actually lowers the mudflat surface.

457 The long-term measurements of sediment accretion and surface elevation change over the
458 duration of the experiment confirm that sedimentation rates at the salt marsh are high
459 compared to the long-term regional SLR rate of ca. 2.23 mm yr^{-1} (for Sheerness (Fig. 1)

during the period 1901 - 2006, reported by Woodworth et al., 2009). The salt marsh therefore appears to represent a healthy tidal wetland with respect to its ability to vertically adapt to rising sea levels. However, the fact that the marsh's apparent ability to adapt to SLR is due to the removal of sediment from the marsh edge and the adjacent tidal mudflat in very close vicinity of the salt marsh edge, shows that the marsh is less resilient to SLR than anticipated from the vertical accretion rates alone (Fig. 9). As a consequence, the mudflat surface is gradually being eroded, interrupted by episodic import events which (partly) replenish the removed sediment with sediment from sources further offshore. This process is particularly observed during periods of high HW levels and low wave activity (Fig. 8).

Sediment deposition on the marsh platform did not show any significant trends in relation to the distance to the marsh edge. One might expect a decrease in sediment deposition rates with increasing distance from the marsh edge (Christiansen et al., 2000; Temmerman et al., 2003; van Proosdij et al., 2006; Poirier et al., 2017), but our data does not show any such trend. Instead, the sediment that is resuspended on the tidal mudflat is distributed into the salt marsh both via the marsh edge and through the complex channel network, leading to uniform sediment deposition within the most seaward 47 m of the marsh. The distribution of suspended sediment this far into the salt marsh is likely related to the wave exposure of the study site, as sediment that is initially deposited on the marsh surface may be resuspended and washed away during the same tide (Ma et al., 2018; Reef et al., 2018). With increasing inland distance, this effect becomes weaker as wave heights and energies are rapidly reduced when travelling over the vegetated marsh surface (Möller and Spencer, 2002).

5.3 Implication for long-term salt marsh morphological development

Previous studies have highlighted the importance of intertidal sediment resuspension as a driver for sediment availability of coastal salt marshes (Schuerch et al., 2013; Schuerch et al., 2014; Ma et al., 2018) and the possibility that vertical sediment accretion may occur through redistribution of sediment from the tidal mudflat and the marsh edge (Mariotti and Carr, 2014). The fact that the deposited sediment is withdrawn from the marsh edge and the mudflat directly adjacent to the marsh edge, however, implies a much stronger negative effect of this sediment redistribution process on the overall morphological development of the salt marsh, if the removed sediment is not entirely replenished (Fig. 9). The coastal slope increases much faster than if the sediments were to originate from the wider tidal mudflat. Such an increased coastal slope inevitably increases the wave heights of incoming waves (Fagherazzi and Wiberg, 2009) and the susceptibility of the salt marsh to landward retreat (Callaghan et al., 2010; Mariotti and Fagherazzi, 2010; Fig. 9).

Based on modelling studies, periods of lateral salt marsh erosion have been suggested either as part of a cyclic behaviour of coastal salt marshes, where erosional phases are followed by vegetation reestablishment and seaward expansion of the marsh (van de Koppel et al., 2005), or as a transition from one stable state to another stable state, after a threshold condition has been exceeded (Mariotti and Fagherazzi, 2010). These thresholds are site dependent in magnitude, but usually depend on the rate of relative SLR, general sediment availability, nearshore bathymetry, sediment characteristics and prevailing wind climate (Mariotti and Carr, 2014).

In our study region (i.e. the Dengie Peninsula), a general trend of lateral marsh retreat (erosion) has been reported since 1953, following an extensive period of rapid expansion between 1870 and 1953 (van der Wal and Pye, 2004). The post-1953-period has been

505 characterized by both periods of very rapid retreat (ca. 16 ha yr^{-1} from 1970 - 1973 and 20 ha
506 yr^{-1} from 1953-1960), times of reduced loss rates (ca. 9 ha yr^{-1} from 1978 and 1981 and ca.
507 2.5 ha yr^{-1} since 1981), and occasionally even slow progradation (Greensmith and Tucker,
508 1965; Harmsworth and Long, 1986; Cooper et al., 2001; van der Wal and Pye, 2004).
509 Currently, our data suggest maximum marsh edge retreat rates of up to 5.5 m yr^{-1} at the widest
510 part of the marsh, falling to 0.8 m yr^{-1} on the transect of this experiment. Unlike the classical
511 erosion of a marsh cliff (van de Koppel et al., 2005; Marani et al., 2011), the lateral erosion
512 of this salt marsh is characterized by the erosion of the ridge-runnel system (Greensmith and
513 Tucker, 1966) as well as the seaward tidal mudflat. The formation and erosion of the ridge-
514 runnel system has been suggested to be part of the cyclic behaviour of marsh edge retreat and
515 progradation, assuming that the sediment removed from the marsh edge during lateral
516 erosion, is deposited on the tidal mudflat in front of the marsh edge, enabling the marsh to
517 re-establish once the mudflat elevation is sufficiently high (Greensmith and Tucker, 1966).

518 Our data, however, show that the majority of the sediment removed from the marsh edge and
519 the mudflat is deposited on the marsh surface, not on the tidal mudflat, suggesting that rather
520 than being a temporary erosional phase, the mudflat-salt marsh system in Tillingham is out
521 of equilibrium with the current physical setting. Based on the available data, we can therefore
522 not conclusively establish whether this instability is part of a cyclic behaviour on decadal
523 timescales or if it indicates the system's adaptation to a new equilibrium with a reduced salt
524 marsh area, in response to an environmental threshold being exceeded. Possible reasons for
525 threshold exceedance are either a reduction in the general sediment availability of the broader
526 coastal environment (e.g. reduction in riverine sediment discharge), a long-term change in
527 longshore sediment transport (e.g. due to changes in the wind/wave climate),

528 geomorphological changes within the broader coastal shelf environment (e.g. shifting
529 subtidal sand ridges and channels in the Greater Thames estuary), or the local SLR rate
530 exceeding the ability of this system to adapt to changes in external forcing.

531 The continuous loss of salt marsh area through lateral erosion despite the high sedimentation
532 rates observed on the marsh surface highlights the close coupling of the sediment dynamics
533 on the tidal mudflat with those on the marsh surface. Salt marsh sedimentation and elevation
534 growth rates alone, often used to assess the ability of salt marshes to adapt to future SLR
535 (Webb et al., 2013), are therefore an unsuitable tool for assessing the response of a salt marsh
536 to SLR. When considering the ability of coastal salt marshes to adapt to global SLR, it is
537 therefore crucially important to not only consider the morphological development of the salt
538 marsh, but the salt marsh should also be considered as part of a coupled tidal mudflat-salt
539 marsh system.

540 **6 Conclusions**

541 On the Dengie Peninsula (UK), sediment availability for the vertical accretion of the marsh
542 has been shown to be highly variable in time and primarily controlled by wave activity. The
543 recorded suspended sediment concentrations are particularly high during moderate to high
544 wave events in the winter months, therefore enabling the marsh to vertically grow at a pace
545 that exceeds the long-term, regional rate of SLR. The contributed sediment, however, has
546 been shown to originate from the marsh edge and the tidal mudflat directly adjacent to the
547 salt marsh, namely within 130 m from the marsh edge (whereas the entire mudflat is 3.7 km
548 wide), causing a lowering of the mudflat surface. The simultaneous increase in marsh
549 elevation and the erosion of the mudflat surface causes an increase in coastal slope and

facilitates lateral marsh edge erosion, a process that has long been observed on this marsh. Our results show that vertical sediment accretion and surface elevation change alone are no indicators of resilience to SLR for coastal salt marshes. Rather, it is necessary to assess the morphological development of the entire tidal mudflat-salt marsh system to understand how resilient a coastal salt marsh really is to environmental forcing.

7 Acknowledgments

We thank Athanasios Vafeidis and Roberto Mayerle from the Christian-Albrechts-University of Kiel ("The Future Ocean" Excellence Cluster) for access to field equipment. At the Department of Geography, Cambridge University we thank Chris Rolfe, Steve Boreham and Adam Copeland for support in conducting field and laboratory data collection; Elizabeth Christie, James Tempest and Ruth Reef for help during data collection in the field; and Iris Möller for her valuable comments.

8 Funding

This work was supported by the German Research Foundation - DFG [grant no: 272052902] and by the Cambridge Coastal Research Unit (Visiting Scholar Programme to MS). Additional support was received from the European Commission under the FP7 project Foreshore Assessment Using Space Technology [grant no: 607131] as well as the NERC-funded projects Coastal Biodiversity and Ecosystem Services Sustainability (CBESS; grant no: NE/J015423/1) and BLUE-coast (grant no: NE/N015878/1).

9 Data Availability

570 Datasets related to this article can be found at *[Link to Mendeley Data]*, an open-source
571 online data repository hosted at Mendeley Data

572 **10 Figure captions**

573 Figure 1: Study area. (A) Location of the study site in southeast England, on the northern
574 margin of the Greater Thames Estuary and (B) distribution of coastal salt marshes (green
575 areas) on the Essex coast, including the location of the study site (red triangle) on the salt
576 marsh near Tillingham.

577 Figure 2: Experimental design. Aerial photograph from 2016 (Environment Agency, 2016b)
578 of the studied salt marsh, the locations of the measurement devices and the topographical
579 profile of the tidal mudflat, the transition to the salt marsh and the seaward part of the
580 vegetated marsh platform, based on a 1 m digital terrain model (Environment Agency,
581 2016a). The seaward turbidity profiler (ASM2113) and ADCP (Nortek Aquadopp Profiler)
582 were moved from position ASM2113_a to ASM2113_b on 03/06/2016. One Solnist pressure
583 sensor was placed at each of the sites ASM2113, ASM2115/P2, P4 and SET2. The pressure
584 transducer PDCR 1830 was located in the transition zone from the tidal mudflat to the
585 vegetated salt marsh.

586 Figure 3: Intertidal sediment resuspension. Relationship between wave proxy and median
587 depth-averaged SSC. Each data point represents one tidal inundation. Data are separated
588 between summer (red squares) and autumn/winter (blue diamonds) measurements.

589 Figure 4: Landward SSC increase. Linear relationship between depth-averaged SSC at
590 ASM2113 (mudflat) and ASM2115 (marsh edge) for the entire measurement period (summer
591 and autumn/winter).

592 Figure 5: Sediment deposition on the salt marsh. Average sediment deposition (g) of all filter
593 traps on the vegetated salt marsh (D: green bars), the maximum SSC (C_{max}: brown line, in
594 mg l^{-1}) and the inundation frequency (IF: blue stars, in tens) at ASM2115 for each sampling
595 period (2 - 10 days, but usually 5 days) between May and December 2016. No samples are
596 available for July and August. Both C_{max} and IF are positively related to D: $D = 0.00049 *$
597 $C_{max} + 0.055 *$ IF ($R^2 = 0.69$, $p < 0.001$).

598 Figure 6: Spatial pattern of average sediment deposition. Boxplot of sediment deposition (g)
599 for all four filter-trap sites (P4, ASM2115, SET1 (during summer), SET2 (during
600 autumn/winter), according to the map in Fig. 2), only accounting for periods, when
601 inundation had occurred during at least one tide. Medians are represented by red lines, blue
602 boxes indicate the 25th and 75th percentile (Q25 and Q75). Outliers (red crosses) are values
603 larger than Q75 + 1.5 * (Q75 - Q25).

604 Figure 7: Spatial patterns of individual sediment deposition events. Sediment deposition (g)
605 from filter traps at four different locations on the salt marsh for every individual sampling
606 period. Bars are shown in the order of the site's distances to the marsh edge: ASM2115 (blue
607 bars): 0 m; P4 (orange bars): 22 m; SET1 (grey bars): 29 m; SET2 (green bars): 43 m. Error
608 bars represent the standard deviation of up to three filters deployed per site. Significant spatial
609 trends of sediment deposition are indicated by red arrows, insignificant trends by "us".

610 Figure 8: Data time series. Time series of meteorological, hydrodynamic, SSC and mudflat
611 morphology data for the entire measurement period. Top panel: prevailing wind conditions
612 (blue: wind speed; red: onshore wind; green: offshore; black: cross-shore). 2nd panel:
613 hydrodynamic forcing (stars: HW levels at ASM2113; crosses: HW levels at ASM2115; solid
614 line: wave proxy at ASM2113; dashed line: smoothed wave proxy (moving average: 10
615 tides). 3rd panel: median SSC (brown squares: ASM2113; green circles: ASM2115). Bottom
616 panel: mudflat morphodynamics (bars: net erosion (negative) and deposition (positive)).

617 Figure 9: Conceptual model. Schematic view of the implications of our data for the long-
618 term morphological development of the salt marsh. The continuous arrow indicates the
619 primary mechanism controlling the temporal variability of sediment supply to the salt marsh,
620 dashed arrows indicate other possible mechanisms for sediment delivery, here found to be
621 insignificant and the dotted arrows indicate the occasional replenishment of the near-edge
622 tidal mudflat from either the lower tidal mudflat or external sources. The expected future
623 topography is indicated by the dashed profile line.

624 **11 Tables**

625 Table 1: Aggregation of high frequency raw data on hydrodynamic forcing and turbidity as

626 well as the morphological data on marsh and mudflat dynamics.

Var. group	**Variable**	**Level of aggregation**		
		Raw data	**Single tidal inundation**	**Sampling period (2 - 10 days, usually 5 days)**
Hydrodynamic forcing	**Still water level (ASM2113)**	Moving-average filter with 15-min window size applied to raw water level data	- Maximum inundation depth (**HW level**) - Tidal asymmetry (ebb / flood duration)	- Mean height of HW levels (**avg. HW level**) - Highest HW level (**max. HW level**) - Inundation frequency (**IF**)
	Wave proxy (ASM2113)	Raw water level data (1/30 Hz)	Mean deviation of raw water level data from still water level (**Wave proxy**)	- Mean wave proxy (**avg. WP**) - Maximum wave proxy (**max. WP**)
	Depth-normalized wave proxy (ASM2113)		Wave proxy divided by HW level (**norm. Wave proxy**)	- Mean normalized wave proxy (**avg. norm. WP**)
Turbidity	**Suspended sediment concentrations (SSC)**	Depth-averaged SSC (1/30 Hz) derived from SSC profiles	Median depth-averaged SSC (**median SSC**)	- Mean of median SSC (**avg. SSC**) - Maximum of median SSC (**max. SSC**)
	Landward SSC increase		Difference in median SSC between the seaward and the landward turbidity profilers (**SSC difference**)	- Mean SSC difference (**avg. SSC difference**) - Maximum SSC difference (**max. SSC difference**)
Marsh and mudflat morphology	**Sediment deposition on salt marsh**	Filter trap data for sampling periods between 2 and 10 days		- Mean sediment deposition for each site and period, including data of all three traps per site (**sediment deposition**) - Mean sediment deposition of all traps for one period (**avg. sediment deposition**)
	Mudflat morphology	Tracer stick data for sampling periods between 2 and 10 days		- Thickness of sediment on top of the eroded tracer stick (**top layer**) - Change in mudflat surface elevation (**erosion** = initial stick length – (remaining stick length + top layer))

627 Table 2: Long-term measurements of the increase in vertical salt marsh elevation (RSET
628 reading) and sediment accretion (MH reading) at the sites SET1 and SET2, derived from the
629 Rod Surface-Elevation Tables (RSET) and the Marker Horizons (MH), respectively.

Date	Site	RSET average (mm)[+]	RSET std.	SET (±1 standard error) rate (mm yr^{-1})	MH average (mm)[+]	MH std.	MH (±1 standard error) rate (mm yr^{-1})
18/12/2015	SET1	0.00	7.86		0.00	5.21	
11/07/2016	SET1	6.89	7.33	**5.6 (±1.5)**	6.83	7.91	**17.4 (±2.4)**
17/02/2017	SET1	6.64	6.90		20.25	7.44	
18/12/2015	SET2	0.00	13.51		0.00	7.39	
11/07/2016	SET2	2.44	11.44	**5.3 (±2.3)**	5.42	6.44	**9.0 (±2.8)**
17/02/2017	SET2	6.19	9.91		10.50	10.13	

630 [+]RSETs and MHs were installed in 2012 - readings reported here were reset to start at zero in
631 December 2015.

632 ## 12 References

633 Allen, J.R.L., 2000. Morphodynamics of Holocene salt marshes: a review sketch from the
634 Atlantic and Southern North Sea coasts of Europe. Quaternary Science Reviews 19, 1155-
635 1231.

636 Allen, J.R.L., Duffy, M.J., 1998. Medium-term sedimentation on high intertidal mudflats and
637 salt marshes in the Severn Estuary, SW Britain: the role of wind and tide. Marine Geology
638 150, 1-27.

639 Andersen, T.J., 2001. Seasonal Variation in Erodibility of Two Temperate, Microtidal
640 Mudflats. Estuarine, Coastal and Shelf Science 53, 1-12.

641 Barbier, E.B., Hacker, S.D., Kennedy, C., Koch, E.W., Stier, A.C., Silliman, B.R., 2011. The
642 value of estuarine and coastal ecosystem services. Ecological Monographs 81, 169-193.

643 Bartholdy, J., Christiansen, C., Kunzendorf, H., 2004. Long term variations in backbarrier
644 salt marsh deposition on the Skallingen peninsula – the Danish Wadden Sea. Marine
645 Geology 203, 1-21.

646 Bellucci, L.G., Frignani, M., Cochran, J.K., Albertazzi, S., Zaggia, L., Cecconi, G., Hopkins,
647 H., 2007. 210Pb and 137Cs as chronometers for salt marsh accretion in the Venice Lagoon

– links to flooding frequency and climate change. Journal of Environmental Radioactivity 97, 85-102.

Bergamino, L., Schuerch, M., Tudurí, A., Carretero, S., García-Rodríguez, F., 2017. Linking patterns of freshwater discharge and sources of organic matter within the Río de la Plata estuary and adjacent marshes. Marine and Freshwater Research, 68, 1704-1715.

Blum, M.D., Roberts, H.H., 2009. Drowning of the Mississippi Delta due to insufficient sediment supply and global sea-level rise. Nature Geoscience 2, 488-491.

Cahoon, D.R., Lynch, J.C., Perez, B.C., Segura, B., Holland, R.D., Stelly, C., Stephenson, C., Hensel, P., 2002. High-Precision Measurements of Wetland Sediment Elevation: II. The Rod Surface Elevation Table. Journal of Sedimentary Research 72, 734-739.

Cahoon, D.R., Reed, D.J., Day, J.W., 1995. Estimating shallow subsidence in microtidal salt marshes of the southeastern United States: Kaye and Barghoorn revisited. Marine Geology 128, 1-9.

Callaghan, D.P., Bouma, T.J., Klaassen, P., van der Wal, D., Stive, M.J.F., Herman, P.M.J., 2010. Hydrodynamic forcing on salt-marsh development: Distinguishing the relative importance of waves and tidal flows. Estuarine, Coastal and Shelf Science 89, 73-88.

Christiansen, T., Wiberg, P.L., Milligan, T.G., 2000. Flow and Sediment Transport on a Tidal Salt Marsh Surface. Estuarine, Coastal and Shelf Science 50, 315-331.

Church, J.A., Clark, P.U., Cazenave, A., Gregory, J.M., Jevrejeva, S., Levermann, A., Merrifield, M.A., Milne, G.A., Nerem, R.S., Nunn, P.D., Payne, A.J., Pfeffer, W.T., Stammer, D., Unnikrishnan, A.S., 2013. Sea Level Change, in: Stocker, T.F., Qin, D., Plattner, G.-K., Tignor, M., Allen, S.K., Boschung, J., Nauels, A., Xia, Y., Bex, V., Midgley, P.M. (Eds.), Climate Change 2013: The Physical Science Basis. Contribution of Working Group I to the Fifth Assessment Report of the Intergovernmental Panel on Climate Change. Cambridge University Press, Cambridge, United Kingdom and New York, NY, USA.

Cooper, N. J., Cooper, T., Burd, F., 2001. 25 years of salt marsh erosion in Essex: Implications for coastal defence and nature conservation. Journal of Coastal Conservation 7, 31-40.

Crosby, S.C., Sax, D.F., Palmer, M.E., Booth, H.S., Deegan, L.A., Bertness, M.D., Leslie, H.M., 2016. Salt marsh persistence is threatened by predicted sea-level rise. Estuarine, Coastal and Shelf Science 181, 93-99.

D'Alpaos, A., Lanzoni, S., Marani, M., Rinaldo, A., 2007. Landscape evolution in tidal embayments: Modeling the interplay of erosion, sedimentation, and vegetation dynamics. Journal of Geophysical Research: Earth Surface 112, F01008.

D'Alpaos, A., Mudd, S.M., Carniello, L., 2011. Dynamic response of marshes to perturbations in suspended sediment concentrations and rates of relative sea level rise. Journal of Geophysical Research: Earth Surface 116, F04020.

Environment Agency, 2016a. LIDAR Tiles Digital Terrain Model (DTM). Environment Agency.

688 Environment Agency, 2016b. Vertical Aerial Photography Tiles - RGBN. Environment
689 Agency.

690 Fagherazzi, S., Wiberg, P.L., 2009. Importance of wind conditions, fetch, and water levels
691 on wave-generated shear stresses in shallow intertidal basins. Journal of Geophysical
692 Research: Earth Surface 114, F03022.

693 Fettweis, M., Sas, M., Monbaliu, J., 1998. Seasonal, Neap-spring and Tidal Variation of
694 Cohesive Sediment Concentration in the Scheldt Estuary, Belgium. Estuarine, Coastal and
695 Shelf Science 47, 21-36.

696 French, J., 2006. Tidal marsh sedimentation and resilience to environmental change:
697 Exploratory modelling of tidal, sea-level and sediment supply forcing in predominantly
698 allochthonous systems. Marine Geology 235, 119-136.

699 French, J.R., 1993. Numerical simulation of vertical marsh growth and adjustment to
700 accelerated sea-level rise, North Norfolk, U.K. Earth Surface Processes and Landforms
701 18, 63-81.

702 French, J.R., Spencer, T., 1993. Dynamics of sedimentation in a tide-dominated backbarrier
703 salt marsh, Norfolk, UK. Marine Geology 110, 315-331.

704 Friedrichs, C.T., Perry, J.E., 2001. Tidal Salt Marsh Morphodynamics: A Synthesis. Journal
705 of Coastal Research, 7-37.

706 Frostick, L.E., McCave, I.N., 1979. Seasonal shifts of sediment within an estuary mediated
707 by algal growth. Estuarine and Coastal Marine Science 9, 569-576.

708 Grabowski, R.C., Droppo, I.G., Wharton, G., 2011. Erodibility of cohesive sediment: The
709 importance of sediment properties. Earth-Science Reviews 105, 101-120.

710 Green, M.O., 2011. Very small waves and associated sediment resuspension on an estuarine
711 intertidal flat. Estuarine, Coastal and Shelf Science 93, 449-459.

712 Green, M.O. and Coco, G., 2014. Review of wave-driven sediment resuspension and
713 transport in estuaries. Reviews of Geophysics 52, 77-117.

714 Greensmith, J.T., Tucker, E.V., 1965. Salt Marsh Erosion in Essex. Nature 206, 606.

715 Greensmith, J.T., Tucker, E.V., 1966. Morphology and evolution of inshore shell ridges and
716 mud-mounds on modern intertidal flats, near Bradwell, Essex. Proceedings of the
717 Geologists' Association 77, 329-IN326.

718 Harmsworth, G.C., Long, S.P., 1986. An assessment of saltmarsh erosion in Essex, England,
719 with reference to the Dengie Peninsula. Biological Conservation 35, 377-387.

720 Hill, T.D., Anisfeld, S.C., 2015. Coastal wetland response to sea level rise in Connecticut
721 and New York. Estuarine, Coastal and Shelf Science 163, 185-193.

722 Janssen-Stelder, B., 2000. The effect of different hydrodynamic conditions on the
723 morphodynamics of a tidal mudflat in the Dutch Wadden Sea. Continental Shelf Research
724 20, 1461-1478.

725 Kirwan, M.L., Guntenspergen, G.R., D'Alpaos, A., Morris, J.T., Mudd, S.M., Temmerman,
726 S., 2010. Limits on the Adaptability of Coastal Marshes to Rising Sea Level. Geophysical
727 Research Letters 37, L23401.

728 Kirwan, M.L., Guntenspergen, G.R.C.F., 2010. Influence of tidal range on the stability of
729 coastal marshland. Journal of Geophysical Research: Earth Surface 115, F02009.

730 Kirwan, M.L., Murray, A.B., 2007. A coupled geomorphic and ecological model of tidal
731 marsh evolution. Proceedings of the National Academy of Sciences 104, 6118-6122.

732 Kolker, A.S., Kirwan, M.L., Goodbred, S.L., Cochran, J.K., 2010. Global climate changes
733 recorded in coastal wetland sediments: Empirical observations linked to theoretical
734 predictions. Geophysical Research Letters 37, L14706.

735 Le Hir, P., Roberts, W., Cazaillet, O., Christie, M., Bassoullet, P., Bacher, C., 2000.
736 Characterization of intertidal flat hydrodynamics. Continental Shelf Research 20, 1433-
737 1459.

738 Ma, Z., Ysebaert, T., Wal, D., Herman, P.M.J., 2018. Conditional effects of tides and waves
739 on short-term marsh sedimentation dynamics. Earth Surface Processes and Landforms,
740 Early view.

741 Marani, M., D'Alpaos, A., Lanzoni, S., Santalucia, M., 2011. Understanding and predicting
742 wave erosion of marsh edges. Geophysical Research Letters 38.

743 Mariotti, G., Carr, J., 2014. Dual role of salt marsh retreat: Long-term loss and short-term
744 resilience. Water Resources Research 50, 2963-2974.

745 Mariotti, G., Fagherazzi, S., 2010. A numerical model for the coupled long-term evolution
746 of salt marshes and tidal flats. Journal of Geophysical Research: Earth Surface 115,
747 F01004.

748 Met Office, 2006. MIDAS: UK Hourly Weather Observation Data. NCAS British
749 Atmospheric Data Centre.

750 Möller, I., 2006. Quantifying saltmarsh vegetation and its effect on wave height dissipation:
751 Results from a UK East coast saltmarsh. Estuarine, Coastal and Shelf Science 69, 337-
752 351.

753 Möller, I., Spencer, T., 2002. Wave dissipation over macro-tidal saltmarshes: Effects of
754 marsh edge typology and vegetation change. Journal of Coastal Research 36, 506–521.

755 Möller, I., Spencer, T., French, J.R., Leggett, D.J., Dixon, M., 1999. Wave Transformation
756 Over Salt Marshes: A Field and Numerical Modelling Study from North Norfolk,
757 England. Estuarine, Coastal and Shelf Science 49, 411-426.

758 Nolte, S., Koppenaal, E.C., Esselink, P., Dijkema, K.S., Schuerch, M., De Groot, A.V.,
759 Bakker, J.P., Temmerman, S., 2013. Measuring sedimentation in tidal marshes: a review
760 on methods and their applicability in biogeomorphological studies. Journal of Coastal
761 Conservation 17, 301-325.

762 Paterson, D.M., Tolhurst, T.J., Kelly, J.A., Honeywill, C., de Deckere, E.M.G.T., Huet, V.,
763 Shayler, S.A., Black, K.S., de Brouwer, J., Davidson, I., 2000. Variations in sediment

764 properties, Skeffling mudflat, Humber Estuary, UK. Continental Shelf Research 20, 1373-
765 1396.

766 Pedersen, J.B.T., Bartholdy, J., 2006. Budgets for fine-grained sediment in the Danish
767 Wadden Sea. Marine Geology 235, 101-117.

768 Poirier, E., van Proosdij, D., Milligan, T.G., 2017. The effect of source suspended sediment
769 concentration on the sediment dynamics of a macrotidal creek and salt marsh. Continental
770 Shelf Research 148, 130-138.

771 Reed, D.J., 1988. Sediment dynamics and deposition in a retreating coastal salt marsh.
772 Estuarine, Coastal and Shelf Science 26, 67-79.

773 Reed, D.J., 1989. Patterns of sediment deposition in subsiding coastal salt marshes,
774 Terrebonne Bay, Louisiana: The role of winter storms. Estuaries 12, 222-227.

775 Reef, R., Schuerch, M., Christie, E.K., Möller, I., Spencer, T., 2018. The effect of vegetation
776 height and biomass on the sediment budget of a European saltmarsh. Estuarine, Coastal
777 and Shelf Science 202, 125-133.

778 Rodríguez, J.F., Saco, P.M., Sandi, S., Saintilan, N., Riccardi, G., 2017. Potential increase in
779 coastal wetland vulnerability to sea-level rise suggested by considering hydrodynamic
780 attenuation effects. Nature Communications 8, 16094.

781 Runte, K., 1989. Methodische verfahren zur quantifizierung von umlagerungen in
782 intertidalen sedimenten. Meyniana 41, 153-165.

783 Schepers, L., Kirwan, M., Guntenspergen, G., Temmerman, S., 2017. Spatio-temporal
784 development of vegetation die-off in a submerging coastal marsh. Limnology and
785 Oceanography 62, 137-150.

786 Schuerch, M., Dolch, T., Reise, K., Vafeidis, A.T., 2014. Unravelling interactions between
787 salt marsh evolution and sedimentary processes in the Wadden Sea (southeastern North
788 Sea). Progress in Physical Geography: Earth and Environment 38, 691-715.

789 Schuerch, M., Spencer, T., Temmerman, S., Kirwan, M.L., Wolff, C., Lincke, D. McOwen,
790 C.J., Pickering, M.D., Reef, R., Vafeidis, A.T., Hinkel, J, Nicholls, R.J., Brown, S., 2018.
791 Future response of global coastal wetlands to sea level rise. Nature 561, 231–234.
792 Schuerch, M., Scholten, J., Carretero, S., García-Rodríguez, F., Kumbier, K., Baechtiger,
793 M., Liebetrau, V., 2016. The effect of long-term and decadal climate and hydrology
794 variations on estuarine marsh dynamics: An identifying case study from the Río de la
795 Plata. Geomorphology 269, 122-132.

796 Schuerch, M., Vafeidis, A., Slawig, T., Temmerman, S., 2013. Modeling the influence of
797 changing storm patterns on the ability of a salt marsh to keep pace with sea level rise.
798 Journal of Geophysical Research: Earth Surface 118, 84-96.

799 Schwarzer, K., Diesing, M., Larson, M., Niedermeyer, R.O., Schumacher, W., Furmanczyk,
800 K., 2003. Coastline evolution at different time scales – examples from the Pomeranian
801 Bight, southern Baltic Sea. Marine Geology 194, 79-101.

802 Shi, B., Wang, Y.P., Du, X., Cooper, J.R., Li, P., Li, M.L., Yang, Y., 2016. Field and
803 theoretical investigation of sediment mass fluxes on an accretional coastal mudflat.
804 Journal of Hydro-environment Research 11, 75-90.

805 Spencer, T., Schuerch, M., Nicholls, R.J., Hinkel, J., Lincke, D., Vafeidis, A.T., Reef, R.,
806 McFadden, L., Brown, S., 2016. Global coastal wetland change under sea-level rise and
807 related stresses: The DIVA Wetland Change Model. Global and Planetary Change 139,
808 15-30.

809 Stevenson, J.C., Ward, L.G., Kearney, M.S., 1986. Vertical accretion in marshes with varying
810 rates of sea level rise, in: Wolfe, D.A. (Ed.), Estuarine Variability. Academic Press Inc.,
811 Orlando, Florida, pp. 241-259.

812 Temmerman, S., Govers, G., Meire, P., Wartel, S., 2003. Modelling long-term tidal marsh
813 growth under changing tidal conditions and suspended sediment concentrations, Scheldt
814 estuary, Belgium. Marine Geology 193, 151-169.

815 Temmerman, S., Govers, G., Wartel, S., Meire, P., 2003. Spatial and temporal factors
816 controlling short-term sedimentation in a salt and freshwater tidal marsh, Scheldt estuary,
817 Belgium, SW Netherlands. Earth Surface Processes and Landforms 28, 739-755.

818 Thieler, E.R., Himmelstoss, E.A., Zichichi, J.L., Ergul, A., 2009. The Digital Shoreline
819 Analysis System (DSAS) Version 4.0 - An ArcGIS extension for calculating shoreline
820 change, Open-File Report, - ed, Reston.

821 Tolhurst, T.J., Consalvey, M., Paterson, D.M., 2008. Changes in cohesive sediment
822 properties associated with the growth of a diatom biofilm. Hydrobiologia 596, 225-239.

823 Towler, P., Fishwick, M., 2017. Reeds Nautical Almanac 2018. Bloomsbury Publishing Plc,
824 London.

825 Underwood, G.J.C., Paterson, D.M., 1993. Seasonal changes in diatom biomass, sediment
826 stability and biogenic stabilization in the Severn Estuary. Journal of the Marine Biological
827 Association of the United Kingdom 73, 871-887.

828 van de Koppel, J., van der Wal, D., Bakker, J.P., Herman, P.M.J., 2005. Self-Organization
829 and Vegetation Collapse in Salt Marsh Ecosystems. The American Naturalist 165, E1-
830 E12.

831 van der Wal, D., Pye, K., 2004. Patterns, rates and possible causes of saltmarsh erosion in
832 the Greater Thames area (UK). Geomorphology 61, 373-391.

833 van Proosdij, D., Davidson-Arnott, R.G.D., Ollerhead, J., 2006. Controls on spatial patterns
834 of sediment deposition across a macro-tidal salt marsh surface over single tidal cycles.
835 Estuarine, Coastal and Shelf Science 69, 64-86.

836 Wang, Y.P., Gao, S., Jia, J., Thompson, C.E.L., Gao, J., Yang, Y., 2012. Sediment transport
837 over an accretional intertidal flat with influences of reclamation, Jiangsu coast, China.
838 Marine Geology 291-294, 147-161.

839 Webb, E.L., Friess, D.A., Krauss, K.W., Cahoon, D.R., Guntenspergen, G.R., Phelps, J.,
840 2013. A global standard for monitoring coastal wetland vulnerability to accelerated sea-
841 level rise. Nature Climate Change 3, 458-465.

842 Weston, N.B., 2014. Declining Sediments and Rising Seas: an Unfortunate Convergence for
843 Tidal Wetlands. Estuaries and Coasts 37, 1-23.

844 Willemsen, P.W.J.M., Borsje, B.W., Hulscher, S.J.M.H., van der Wal, D., Zhu, Z., Oteman,
845 B., Evans, B., Möller, I., Bouma, T.J., 2018. Quantifying Bed Level Change at the
846 Transition of Tidal Flat and Salt Marsh: Can We Understand the Lateral Location of the
847 Marsh Edge? Journal of Geophysical Research: Earth Surface 123. [doi:
848 10.1029/2018JF004742]

849 Woodworth, P.L., Teferle, F.N., Bingley, R.M., Shennan, I., Williams, S.D.P., 2009. Trends
850 in UK mean sea level revisited. Geophysical Journal International 176, 19-30.

851 Zhou Z., Ye Q., Coco G., 2016. A one-dimensional biomorphodynamic model of tidal flats:
852 Sediment sorting, marsh distribution, and carbon accumulation under sea level rise.
853 Advances in Water Resources 93, 288-302.

854 Zhu, Q., Yang, S., Ma, Y., 2014. Intra-tidal sedimentary processes associated with combined
855 wave–current action on an exposed, erosional mudflat, southeastern Yangtze River Delta,
856 China. Marine Geology 347, 95-106.

Figure 1

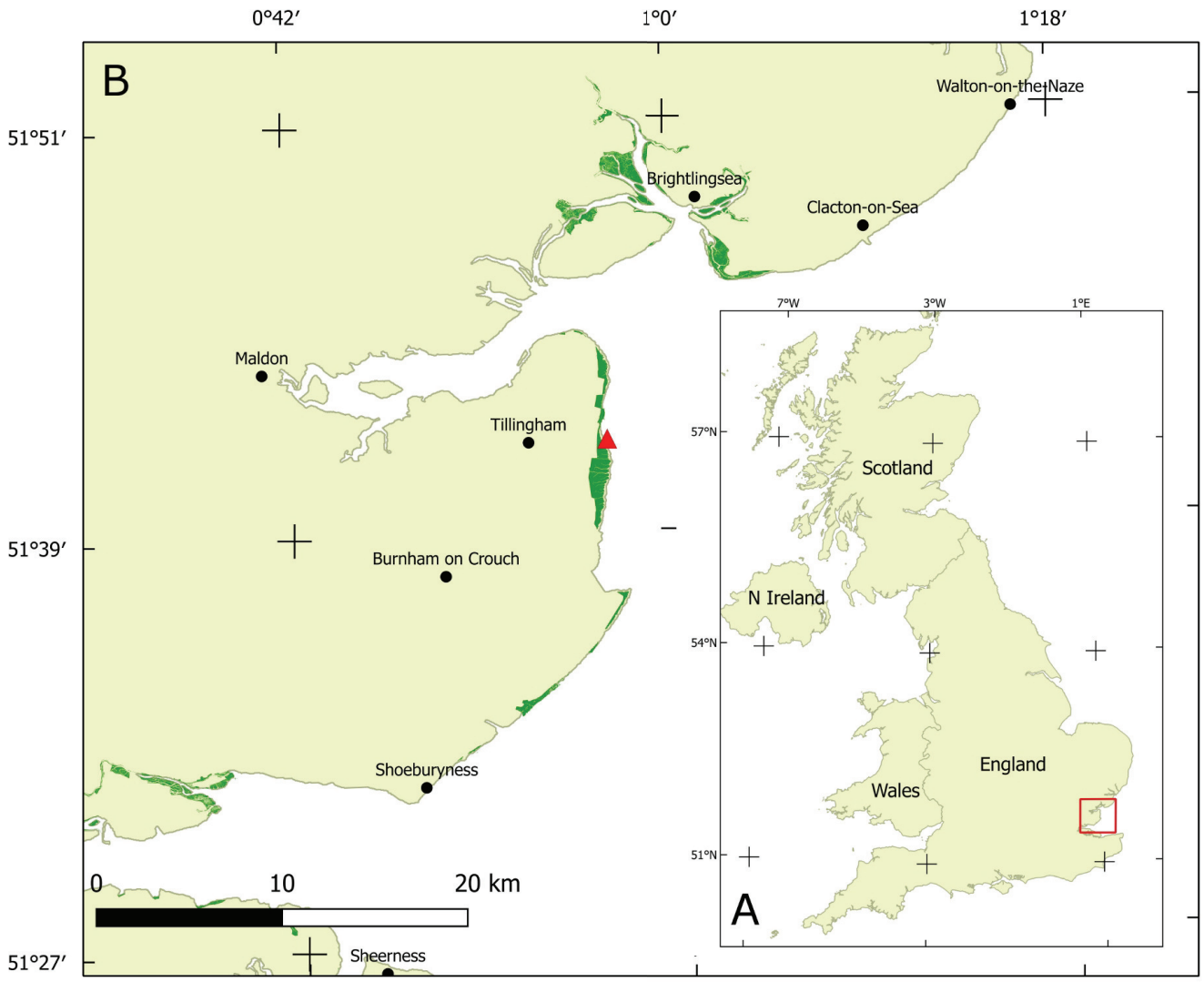
0°42′
1°0′
1°18′
51°51′
51°39′
51°27′
B
Walton-on-the-Naze
Brightlingsea
Clacton-on-Sea
Maldon
Tillingham
Burnham on Crouch
Shoeburyness
Sheerness
0
10
20 km
7°W
3°W
1°E
57°N
54°N
51°N
Scotland
N Ireland
England
Wales
A

Figure 2

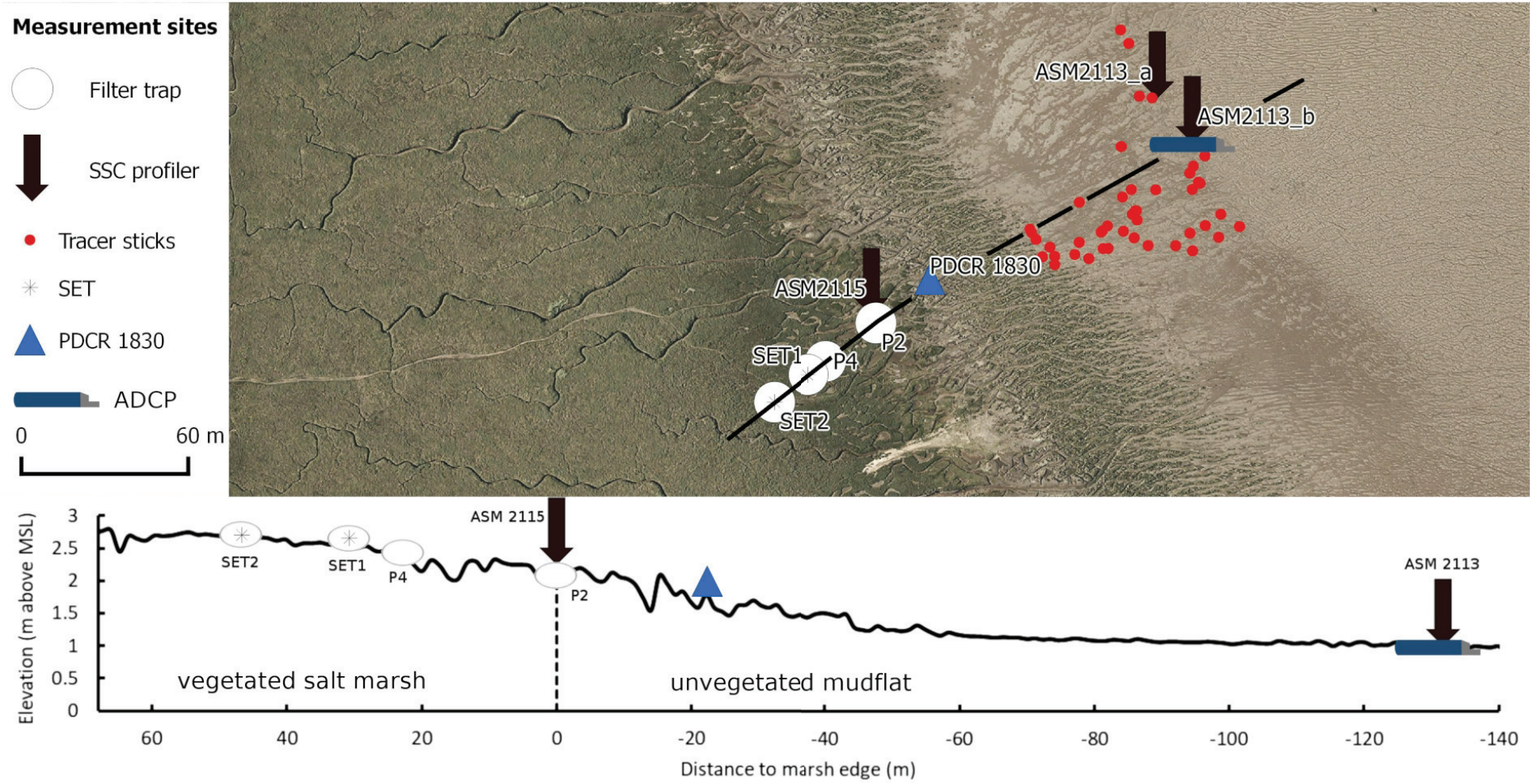
Measurement sites
Filter trap
SSC profiler
Tracer sticks
SET
PDCR 1830
ADCP
0
60 m
ASM2113_a
ASM2113_b
PDCR 1830
ASM2115
P2
SET1
P4
SET2
ASM 2115
SET2
SET1
P4
P2
ASM 2113
vegetated salt marsh
unvegetated mudflat
Elevation (m above MSL)
3
2.5
2
1.5
1
0.5
0
60
40
20
0
-20
-40
-60
-80
-100
-120
-140
Distance to marsh edge (m)

Figure 3

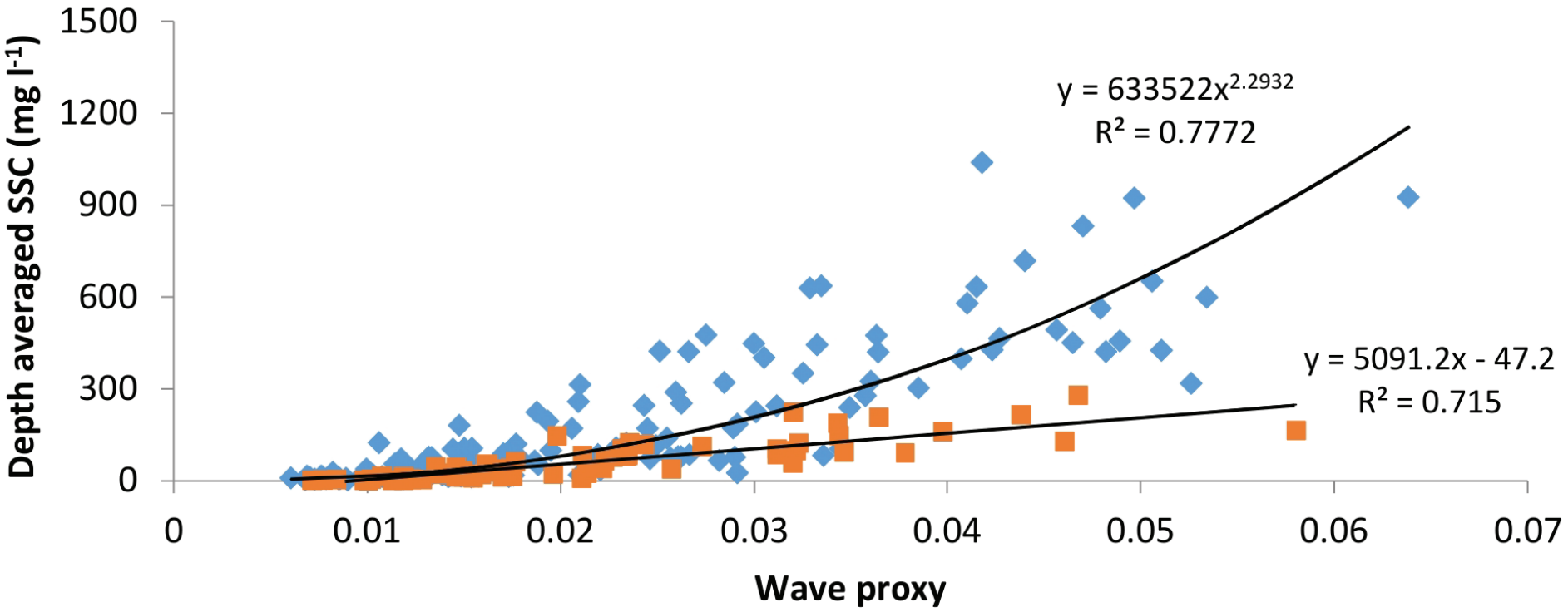
Depth averaged SSC (mg l-1)
1500
1200
900
600
300
0
0
0.01
0.02
0.03
0.04
0.05
0.06
0.07
Wave proxy
y = 633522x2.2932
R² = 0.7772
y = 5091.2x - 47.2
R² = 0.715

Figure 4

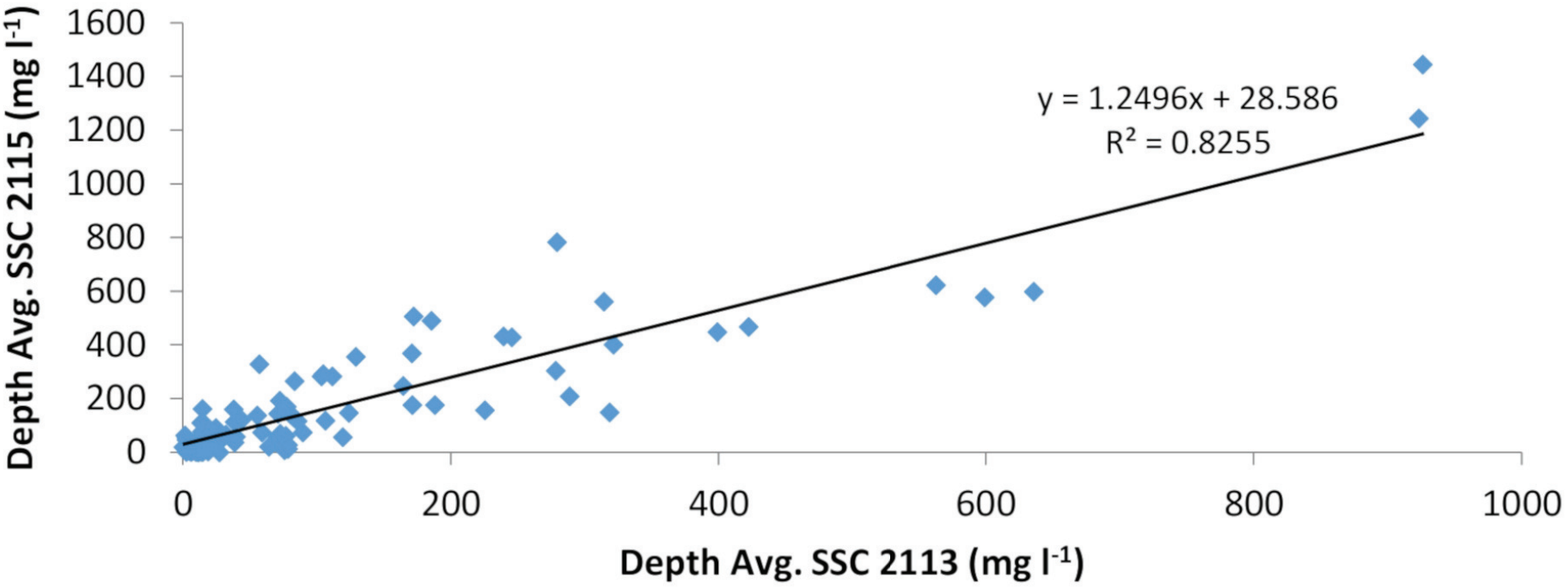
Depth Avg. SSC 2115 (mg l-1)
1600
1400
1200
1000
800
600
400
200
0
0
200
400
600
800
1000
Depth Avg. SSC 2113 (mg l-1)
y = 1.2496x + 28.586
R² = 0.8255

Figure 5

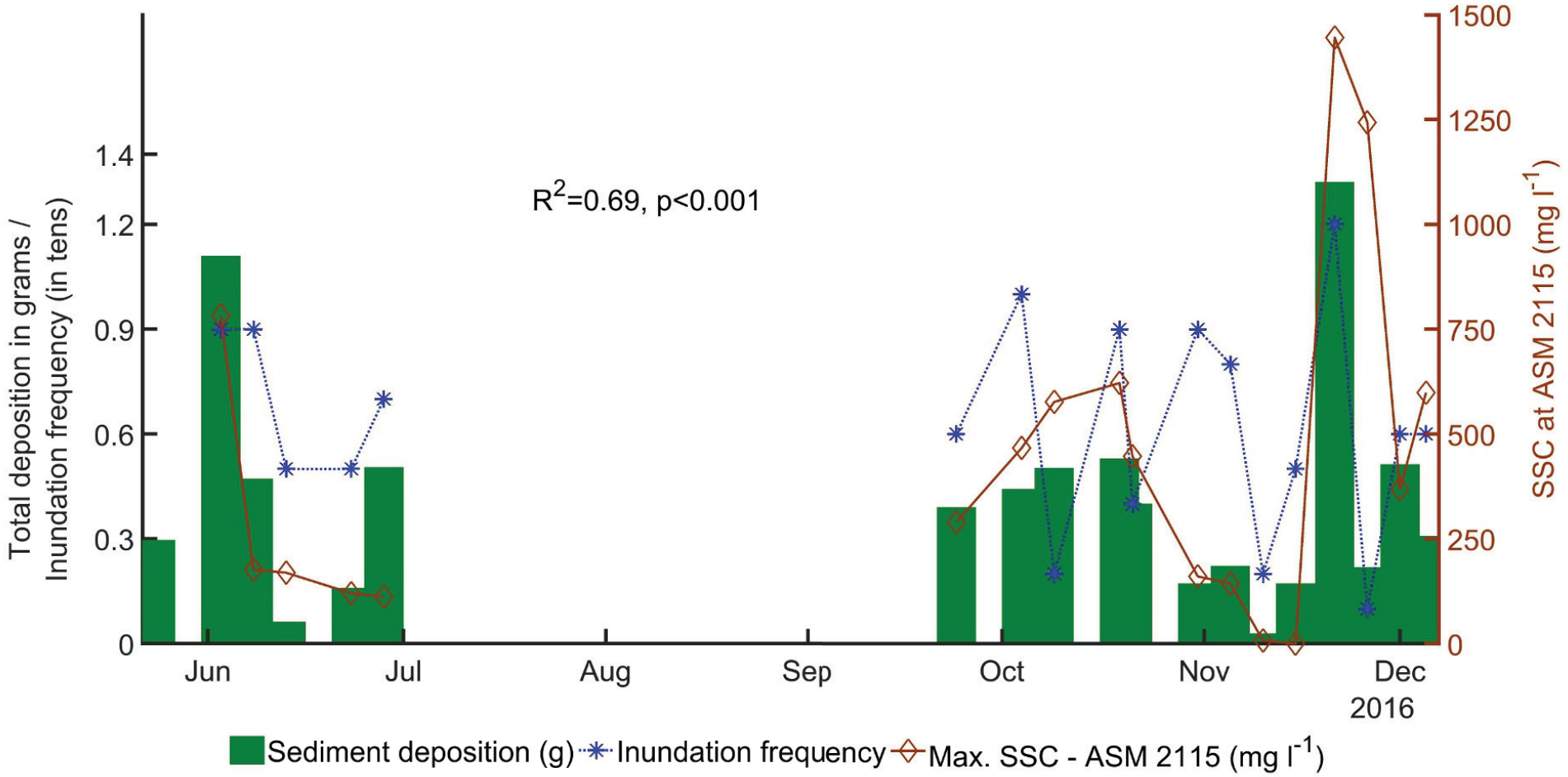
Total deposition in grams / Inundation frequency (in tens)
SSC at ASM 2115 (mg l-1)
R2=0.69, p<0.001
0
0.3
0.6
0.9
1.2
1.4
0
250
500
750
1000
1250
1500
Jun
Jul
Aug
Sep
Oct
Nov
Dec
2016
Sediment deposition (g)
Inundation frequency
Max. SSC - ASM 2115 (mg l-1)

Figure 6

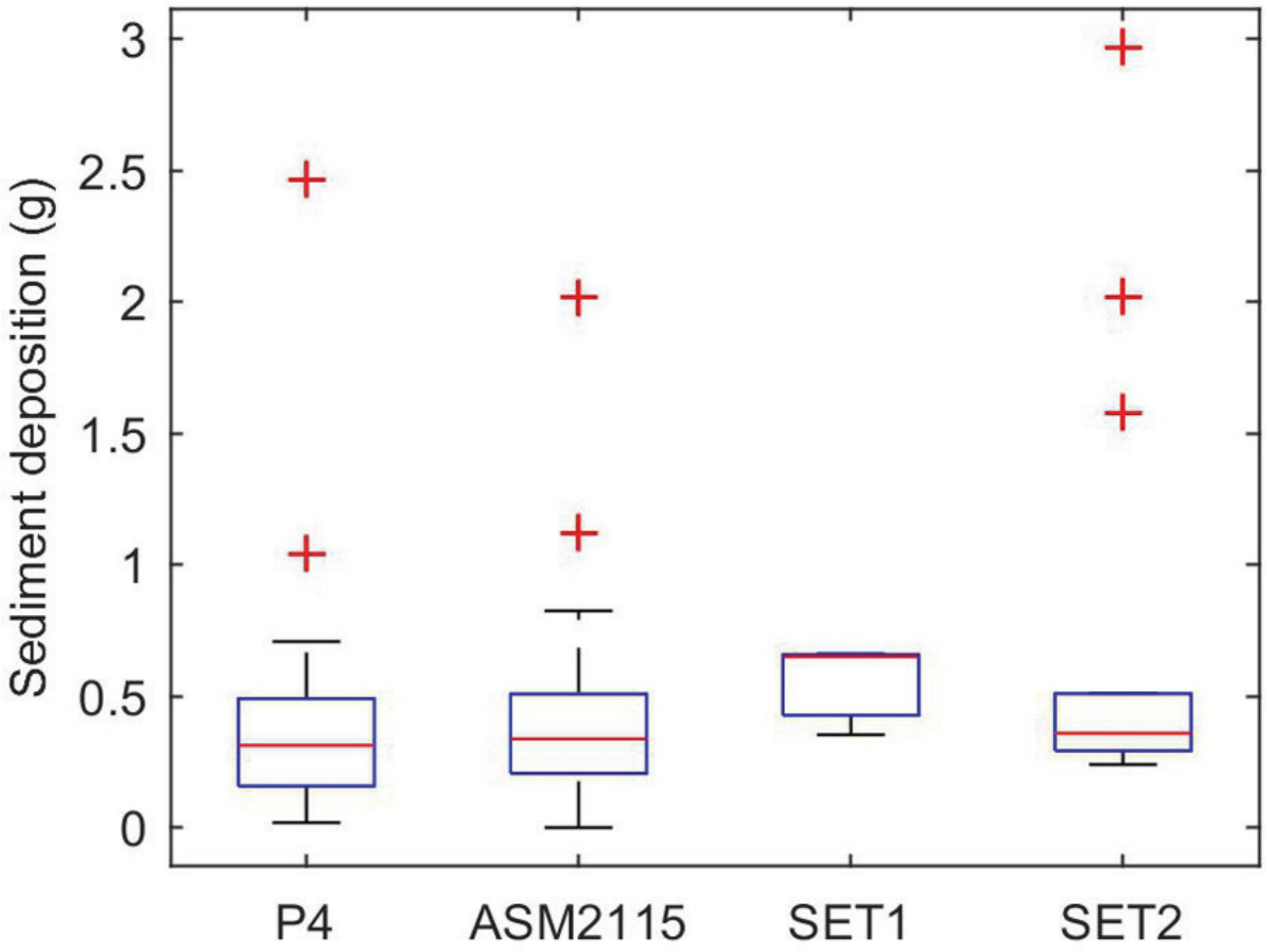

Figure 7

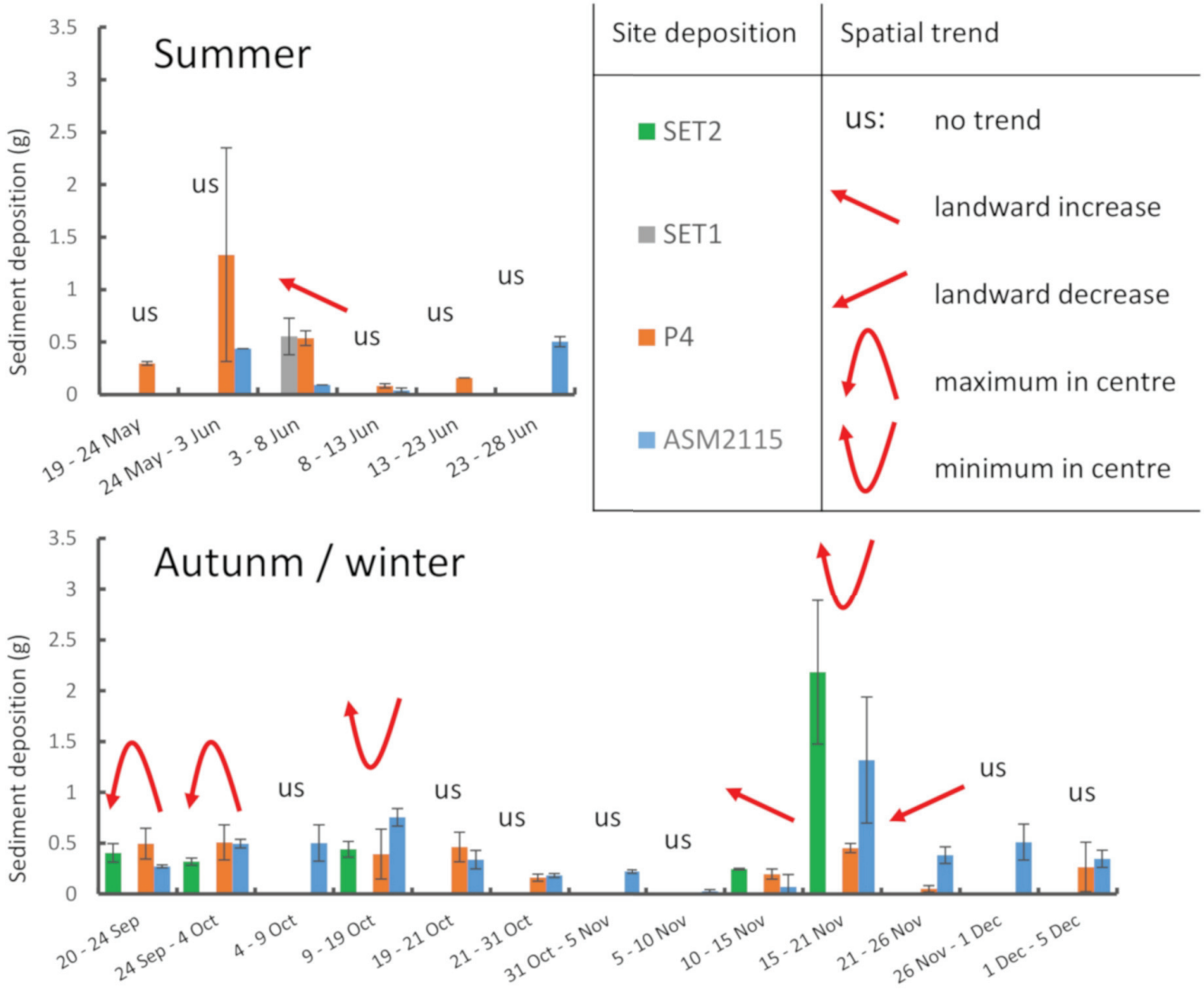
Summer
Sediment deposition (g)
3.5
3
2.5
2
1.5
1
0.5
0
us
us
us
us
us
19 - 24 May
24 May - 3 Jun
3 - 8 Jun
8 - 13 Jun
13 - 23 Jun
23 - 28 Jun
Site deposition
SET2
SET1
P4
ASM2115
Spatial trend
us: no trend
landward increase
landward decrease
maximum in centre
minimum in centre
Autunm / winter
Sediment deposition (g)
us
us
us
us
us
us
us
20 - 24 Sep
24 Sep - 4 Oct
4 - 9 Oct
9 - 19 Oct
19 - 21 Oct
21 - 31 Oct
31 Oct - 5 Nov
5 - 10 Nov
10 - 15 Nov
15 - 21 Nov
21 - 26 Nov
26 Nov - 1 Dec
1 Dec - 5 Dec

Figure 8

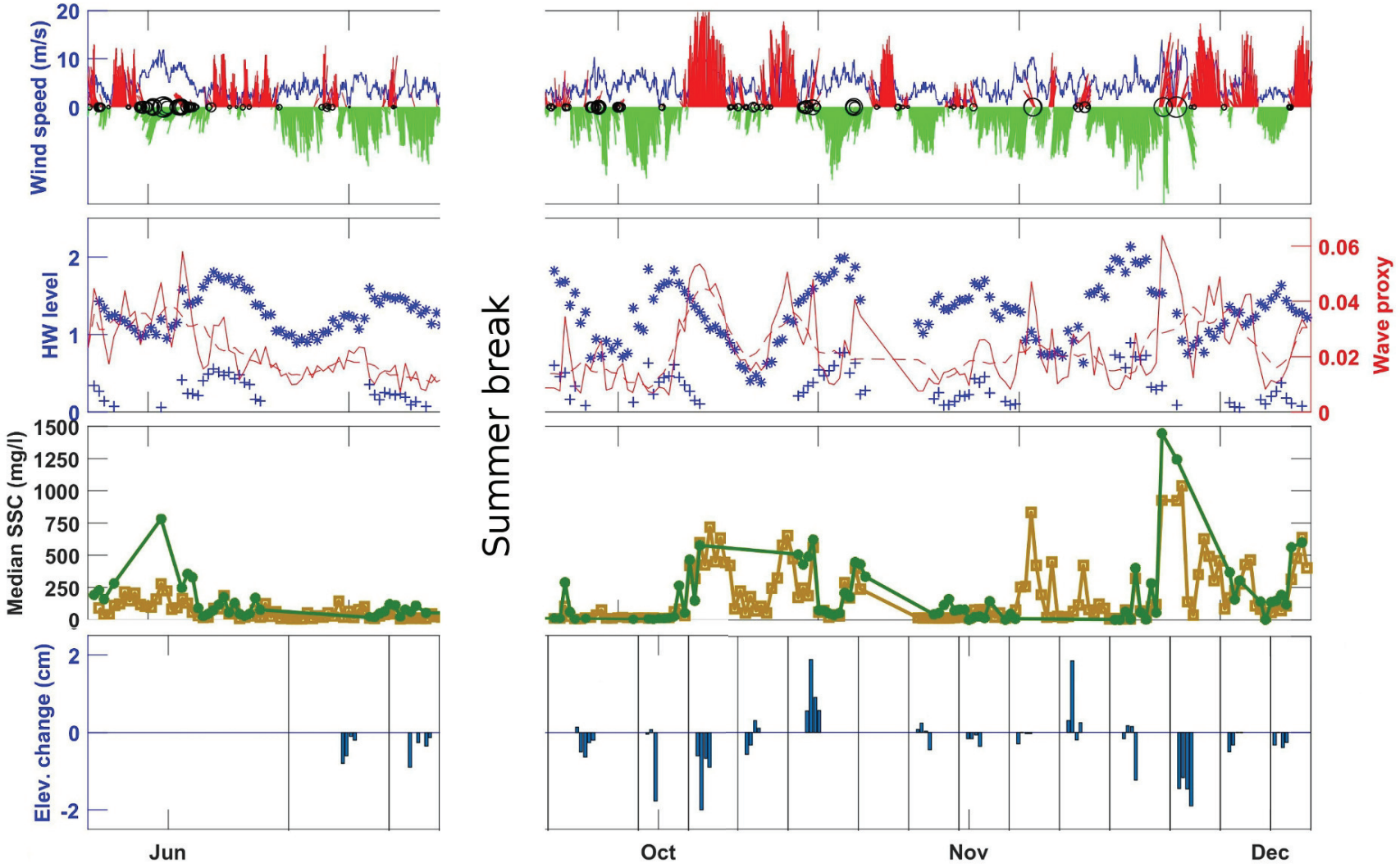
Wind speed (m/s)
20
10
0
HW level
2
1
0
0.06
0.04
0.02
0
Wave proxy
Median SSC (mg/l)
1500
1250
1000
750
500
250
0
Elev. change (cm)
2
0
-2
Summer break
Jun
Oct
Nov
Dec

Figure 9

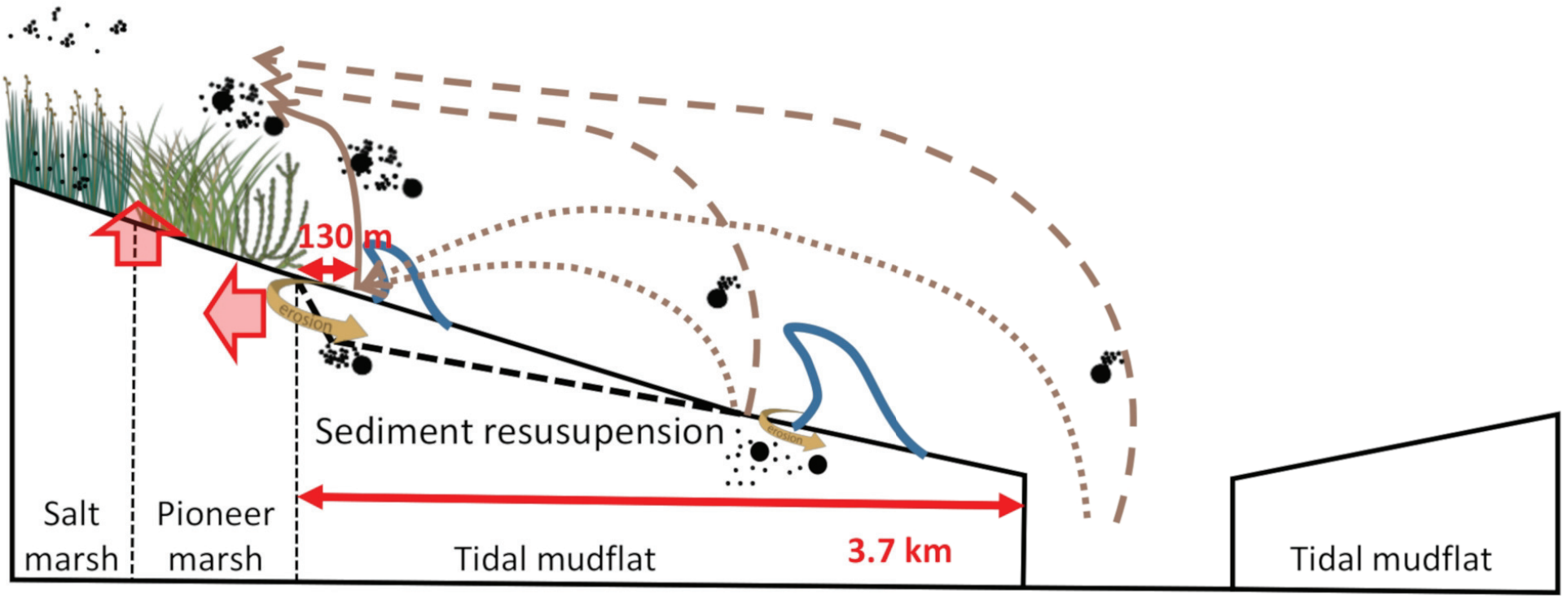
130 m
erosion
erosion
Sediment resusupension
Salt marsh
Pioneer marsh
Tidal mudflat
3.7 km
Tidal mudflat